Title of Document: FABRICATION OF SOFT, FERROMAGNETIC FILMS AND DEVICES AND THEIR PROPERTIES, PRINTABILITY, AND APPLICATIONS

Elizabeth Carlson, Anson Chen, Stephen Chung, Anjali Dhamsania, William Mah, Lillian Mueller, Arjun Sivarajan, and John Ting

Thesis directed by: Dr. Siddhartha Das

Department of Mechanical Engineering

University of Maryland, College Park

Abstract

Materials enabling fabrication of multifunctional devices are a cornerstone of present-day materials science and engineering. Multifunctionality enables use for novel applications in fields like energy, health, sensing, etc. We conducted an extensive literature review into the development of one material capable of multifunctional device fabrication, elastic magnetic films and devices, which have two notable properties: magnetizability, and physical softness and compliance. We highlighted materials, fabrication, characterization, and resulting interactions harnessed to develop inks used to fabricate these films, as well as broadscale applications. We also experimented with an Fe_3O_4-PDMS compliant magnetic film to characterize magnetic properties under modes of deformation. Through bending and twisting, the magnetic saturation, coercivity, and retentivity were measured. Results revealed that bent configurations preserved magnetic characteristics better than twisting configurations; out of tested twisting angles, a 180° rotation displayed properties closest to the undeformed state. We concluded by describing the potential of future research endeavors.

Fabrication of Soft, Ferromagnetic Films and Devices, and their Properties, Printability, and Applications

By

Team GECKO

Elizabeth Carlson

Anson Chen

Stephen Chung

Anjali Dhamsania

William Mah

Lillian Mueller

Arjun Sivarajan

John Ting

Thesis submitted in partial fulfillment of the requirements of the Gemstone Program,
University of Maryland, College Park 2022

Advisory Board:
Dr. Siddhartha Das
Dr. Po-Yen Chen
Dr. Kevin Daniels
Dr. Eleanora Tubaldi
Dr. Ganesh Sriram

I. Acknowledgements

We would like to thank our mentor, Dr. Siddhartha Das, for his counsel and assistance in our research process; none of this would be possible without his unwavering support and the countless resources he has provided. In addition, we are grateful to all of the staff in the Gemstone Honors Program for helping us create and execute an undertaking of this magnitude. We are especially thankful for the indispensable guidance provided by Mr. Swarup Subudhi, Mr. Beihan Zhao, and Mr. Bhargav Chava, and are grateful for their invaluable knowledge, feedback, and caring attitude towards our team. We thank our librarians, Dr. Sarah Over and Mr. Preston Tobery, as well as all of our discussants, for taking the time to review our final thesis and provide thoughtful feedback. Finally, we thank our friends and family for their generous support and encouragement, making all of this research possible.

II. Table of Contents

III. List of Tables

The following table provides a list of figures in this paper and a brief description of their relevance to the paper.

Table	Brief Description
1	A list of tables used in this paper
2	A list of figures used in this paper
3	A list of acronyms (and their meanings) used in this paper
4	Calculated Young's Modulus values from the experiment conducted by Wang *et al.* [1]
5	Saturation Magnetizations of different samples of magnetic films with both low and high iron oxide concentration orientations for different film orientations
6	Latent Magnetizations of different samples of magnetic films with both low and high iron oxide concentration orientations for different film orientations.
7	Coercivity of different samples of magnetic films with both low and high iron oxide concentrations for different film orientations.

Table 1. A list of tables used in this paper.

IV. List of Figures

The following table provides a list of figures in this paper and a brief description of their relevance to the paper.

Figure	Brief Description
1	Schematic describing an overview of the two necessary parts of physically soft magnetic films
2	Schematic describing an overview of the two classifications of fabrication methods to develop magnetic films.
3	Examples of magnetically controlled robots fabricated using additive manufacturing processes
4	Schematic describing an overview of the different characterizations of the thin magnetic films and the properties exhibited by them
5	[Reproduced] Plot showing the range of Young's modulus values of various ferromagnetic and weakly magnetic materials embedded in different polymer matrices
6	M-H curves of sample 1 of the high iron concentration, demonstrating hysteresis, both (a) and (b) show the same data, where (b) is focused on the origin
7	Saturation Magnetization results for samples in varying deformations
8	Latent Magnetization results for samples in varying deformations
9	Coercivity results for samples in varying deformations
10	Schematic depicting motion-inducing structures in microorganisms and the corresponding biomimetic elasto-magnetic microdevices
11	Schematic of microbots that have been shown with the several methods of microcilia-based propulsion

Table 2. A list of figures used in this paper.

V. List of Abbreviations

The following table provides a list of acronyms and their explanations to this paper.

Nomenclature or Acronyms	Meaning
PEG	Polyethylene glycol
PEGA	Poly(ethylene glycol) acrylate
PEGDA	Poly(ethylene glycol) diacrylate
EGDMA	Ethylene glycol dimethacrylate
MAA	Methacrylic acid
PLA	Polylactic acid
PnBA	Poly(n-butylacrylate)
OA	Oleic acid
SEM	Scanning Electron Microscopy
TEM	Transmission Electron Microscopy
PDMS	Polydimethylsiloxane
NP	Nanoparticle
XRD	X-ray Powder Diffraction
MEMS	Microelectromechanical Systems

Table 3. A list of acronyms (and their meanings) used in this paper.

VI. Introduction

The purpose of this thesis is to describe the efforts of Team GECKO during the past two years. During this time, Team GECKO has submitted a review paper titled *Physically Soft Magnetic Films and Devices: Fabrication, Properties, Printability, and Applications* to the Journal of Materials Chemistry C. Recently, this paper was accepted for publication. Team GECKO has also studied the magnetic properties of soft magnetic films fabricated by Swarup Subudhi, a PhD student in the laboratory of Dr. Siddhartha Das.

During the process of writing the review paper, Team GECKO read about the materials and processes used to fabricate soft magnetic films, the processes used to characterize soft magnetic films, and the applications of soft magnetic films. A summary of these facts compiled during this process are included in this thesis.

In collaboration with Swarup Subudhi, Team GECKO recorded the M-H curves of soft magnetic films subjected to different forms of deformation. The purpose of these measurements was to demonstrate the robustness of these films and their suitability for a wide range of applications including microrobotics. These results are included in this thesis.

VII. Literature Review

The contents of this section have been published in the Journal of Materials Chemistry C in a paper written by the authors of this work, as described above.

VII. A. Materials

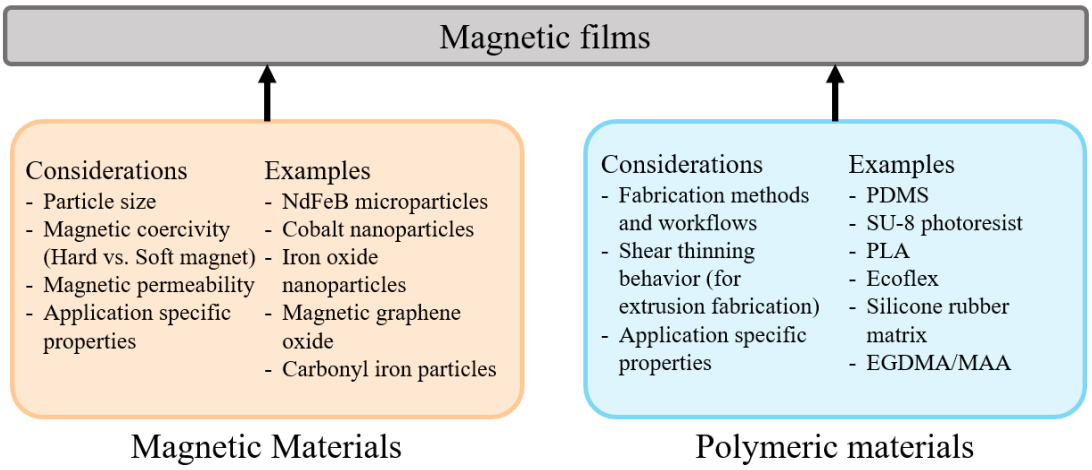

Figure 1. Schematic describing an overview of the two necessary parts of physically soft magnetic films. The left side describes the considerations when selecting a magnetic particle to give the film its magnetic property, as well as several examples of previously used particles. The right side describes the considerations when selecting a polymer material to give the film its physical softness, as well as several examples of previously used polymer materials.

In this section, we will discuss the common materials used in the fabrication of soft, magnetic films, typically involving a polymer matrix and magnetic microparticles or magnetic nanoparticles of various sizes. Materials selected must meet certain requirements to ensure the desirable properties of the physically soft, magnetic films. For example, for the case of the polymer matrix, a low elastic modulus (of the same order as that of the elastomers or even

smaller) is desired for ensuring that the fabricated magnetic films are soft and pliable. Of course, such softness and pliability of the fabricated magnetic films also depend on the aspect ratio of the film [2]. Similarly, the fabricated films must experience a minimum deflection without fracture. Polymers must also have a low glass transition temperature (T_g): ideally this transition temperature should be smaller than the room temperature to ensure the desired flexibility [3].

The polymer materials that are responsible for attributing the desired "softness" and compliance to these films include polydimethylsiloxane (PDMS) [1], [4]–[18], SU-8 photoresist [19], polylactic acid (PLA) [20], Ecoflex 00-10 polymer [21], silicone rubber matrix [22], EGDMA/MAA [23]–[26], poly(n-butylacrylate) (PnBA) [27], [28], poly(ethylene glycol) (PEG) [29], poly (ethylene glycol) acrylate (PEGA) [30], poly(ethylene glycol)diacrylate (PEGDA) [30], etc.

The most common type of polymer material for mechanically soft magnetic inks, PDMS, is often used in conjunction with other materials. It is often used due to its low cost and compatibility with biological applications [31]. PDMS also has well established workflows for several fabrication methods such as lithography and its shear thinning behavior opens possible applications in additive manufacturing. Other materials have also been used in conjunction with magnetic microparticles or nanoparticles to achieve other desired properties.

Just like the polymeric materials, there have been several different permutation-combinations on the microparticles or nanoparticles used to fabricate physically soft and magnetically responsive films and inks. For example, the typical microparticles or nanoparticles that are responsible for inducing magnetic actuation capabilities include ferrite nanoparticles [4]–[8], [10], [19], [23], [24], [27], [29], [30], [32]–[36], neodymium-iron-boron (NdFeB)

nanoparticles [1], [9], [11]–[15], [21], [22], magnetic graphene oxide [25], [37], cobalt [38], carbonyl iron particles [39], etc. In order to meet the magnetizability requirement, films must have a high enough volume fraction of magnetic nanoparticles to have a relatively high magnetic moment and experience torque when an external magnetic field is applied. However, having too large of a volume fraction of magnetic nanoparticles can increase the elastic modulus of the film and reduce its flexibility [40]. The magnetic nanoparticles used in the fabrication of such films have been both soft and hard magnets, such as ferrite and NdFeB magnets respectively, depending on their uses. Hard magnets will retain their magnetized direction, but soft magnets can easily be magnetized and demagnetized. Other particles are also used for application specific properties, such as magnetic graphene oxide being selected as the magnetic particle due to its large surface area [25] or ability to be optically stimulated for drug delivery applications [37]. Generally, iron oxide nanoparticles are most commonly used due to their low cost, small size, and their superparamagnetic property [15].

The typical diameter of the iron oxide NPs, which are the most common type of NPs used to fabricate such soft, magnetic films, range from 6nm to 10μm [1], [4]–[8], [19], [23], [24], [27], [29], [30], [34], [36]. Pirmoradi *et al.* [5] used both uncoated iron oxide particles as well as particles coated by a proprietary fatty acid (EMG 1200) and a proprietary hydrophobic surfactant (EMG 1400). Such coatings serve as stabilizers that prevent the NPs from aggregating by overcoming the large NP-NP attractive van der Waals forces. For example, several groups have used iron-oxide particles stabilized with a coating of oleic acid [26], [29], [34], [41]. Others have also used gold NPs for a similar purpose [42]. In addition to such iron-oxide NPs, microscale NdFeB particles have also been used. These particles ranged from 5μm to 70μm in diameter [1], [9], [11]–[15], [21], [22]. For example, the experiments done by Wang *et al.* [1] used NdFeB

particles whose dimensions were between 20μm and 70μm, while Iacovacci *et al*. [15] considered NdFeB particles of dimensions ranging from 5μm to 10μm.

There is a large space of materials commonly used, but the specific fabrication process used often determines the choice of materials (and hence the desirable properties of these materials). For example, for cases where additive manufacturing (such as direct ink writing) methods are used to fabricate the soft, magnetic films, one must ensure that polymer and NPs are chosen so that the magnetic nanocomposite ink demonstrates shear thinning behavior. For such nanocomposite inks, the shear thinning behavior implies that the viscosity must be low enough to ensure that the ink can be extruded out of the nozzle, while at the same time in absence of any pressure (i.e., immediately after printing), the deposited ink volume must retain its shape. The ink must also contain a large volume fraction of a colloid to minimize drying induced shrinkage, which can impart compressive stress on the resulting structures [43].

VII. B. Fabrication

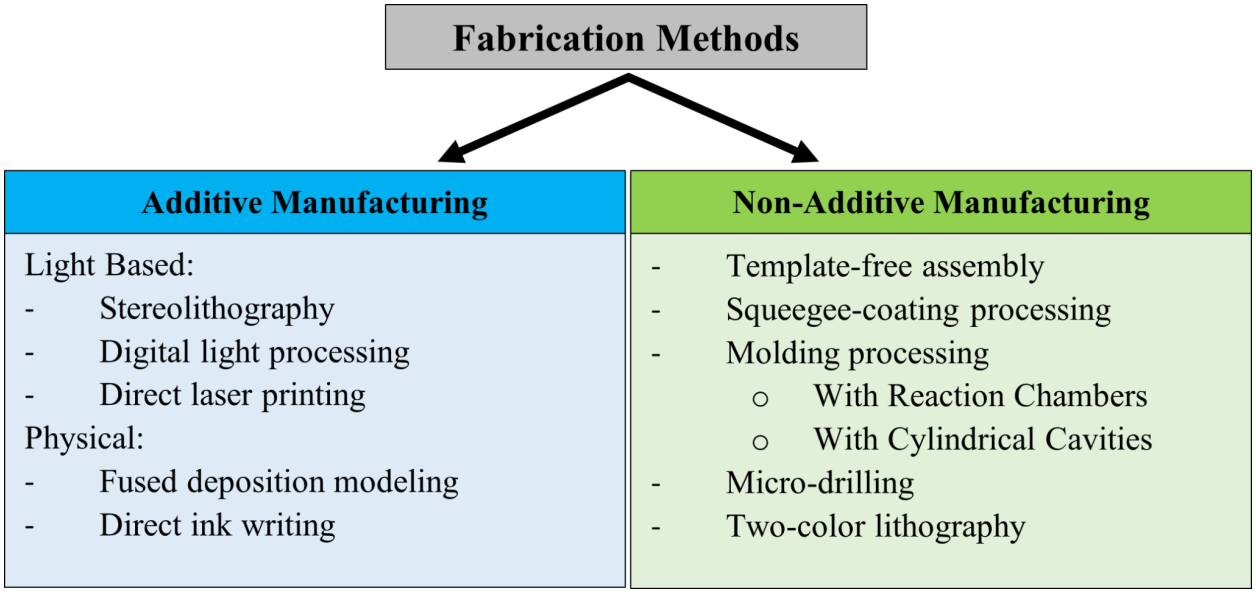

Figure 2. Schematic describing an overview of the two classifications of fabrication methods to develop magnetic films. The left side describes the additively manufactured techniques that will be discussed further in the section. The right side highlights examples of traditional, non-additively manufactured fabrication techniques.

In fabricating magnetizable films, there are two broad categories of methods: non-additive fabrication methods and additive fabrication methods. We will discuss the advantages and disadvantages that each of these methods have.

The first group consists of traditional processes that do not use additive manufacturing. This group of methods is extremely diverse, however the most widely used method by a wide margin is molding. Other methods include template-free assembly and roll-pulling. These methods generally do not require special properties such as photosensitive curing or rheological requirements, unlike additive manufacturing methods.

In the second group, additive manufacturing processes construct 3D structures incrementally, usually layer by layer. These can be divided into light-based methods like stereolithography (SLA), digital light processing (DLP), and direct laser writing (DLW) as well as physical-based methods like fused deposition modeling (FDM), direct ink writing (DIW), and binder jetting.

VII. B. i. Non-Additively Fabricated Soft, Magnetic Films

Traditionally, non-additive strategies have been employed for fabricating soft, magnetic thin films, while additive manufacturing has arisen in popularity in recent years. An evaluation of some of those traditional methods and their effects on various film properties is discussed below.

The first step in the fabrication of soft, magnetic films is to ensure that the dispersed magnetic NPs do not aggregate. To prevent aggregation, for cases where external coating (as described above) is absent or is unable to serve as strong-enough stabilizer, the magnetic nanoparticles are often mixed with a dispersion agent such as toluene [5] or Pluronic F-127 [44], and then sonicated. For example, in the study by Pirmoradi *et al.* [5], to prevent the irreversible aggregation of the iron oxide NPs, dry coated NPs were successively dissolved in toluene at 35°C, stirred, and sonicated in an ultrasound bath for 30 minutes before being mixed with the PDMS prepolymer. However, when using uncoated iron oxide NPs, the procedure requires approximately 4-6 hours of sonication to prevent irreversible aggregation of the NPs, much longer than the time required for dry coated NPs. Thus, during the initial fabrication steps, this confirms that coating the NPs prior to mixing improves both efficiency of the process, as well as prevents significant aggregation.

Template-free assembly is a very common approach in the development of material systems like magnetic films. Timonen *et al.* [38] applied the facile bottom-up approach, based on template-free assembly, for fabrication of magnetically responsive cilia. In this technique, magnetic cilia formed spontaneously from a suspension of micrometer-sized ferromagnetic particles and an elastomeric polymer, all cured in the presence of an external magnetic field. The magnetic suspension was prepared by mixing about 20 mg of the ferromagnetic nanoparticles into 8mL of a liquid solvent containing 30 mg of dissolved elastomeric polymer as the nanoparticles. The suspension was vigorously ultrasonicated for a few minutes and poured into a polytetrafluoroethylene (PTFE) dish with a flat substrate at the bottom. This method does produce a significant amount of aggregation seconds after ultrasonication, however, placing the dish in the magnetic field seems to prevent further aggregation. Utilizing the same approach, Sun and Zheng [45] demonstrated that within this magnetic field, the particles instantaneously formed conical high-aspect-ratio structures, while the polymer remained in its dissolved form. The formation of conical shapes during phase separation can be attributed to the fact that the particle phase is made of cone-like shapes whose aspect ratios resemble cilia. Furthermore, after evaporation, the cones indicated high flexibility, and could be bent by a mechanical force to be set into their final structures. Overall, this method, while it produces aggregates rather quickly, has its advantages in its ability to fabricate mechanically strong strong and flexible films even after magnetic curing is complete. As a result of the robustness of the films produced, template-free assembly is favorable for several combinations of solvents, polymers, and ferromagnetic particles, but particularly constituents in the micrometer and submicrometer size range.

Wang *et al.* [1] used a fabrication method termed "squeegee-coating processing," which is similar to molding processing. Initially, the photoresist was used to form a die, and then a mixture of PDMS and magnetic powder was poured onto the die on a silicon wafer. A transparent film was lowered onto the mixture to eliminate surface bubbles, and then the entire die/mixture/transparency film stack was clamped together. Next, the stack was placed in a vacuum oven to cure the PDMS. The issue with the molding process was that it produced too many bubbles at the surface. Instead of clamping the stack to reduce these bubbles, the squeegee processing method scraped a piece of glass with a flat smooth edge across the die. This method demonstrated success in (and thus is valid for) producing uniform magnetic films ranging in thickness from 40μm to over 200μm, and improved on the molding process in that it significantly reduced air bubbling. Furthermore, this fabrication method produced films with Young's Modulus values between 2.26 MPa to 28.90 MPa, a residual magnetic moment approximating $8.081 \cdot 10^{-5}$ $A \cdot m^2$, and a maximum deflection in a 0.21 T magnetic field of 125 μm. Based on these results, the research suggests that this method is best suited for fabricating a film for micropumps and other microdevice applications that focus on bi-directional motion, large driving forces, and large deflection.

Molding processes are quite popular in the fabrication of magnetic composite films and solve many of the problems stemming from aggregation and bubbling. Rahbar *et al.* [16] and Chen *et al.* [11], in particular, both discussed the direct fabrication of magnetic nanoparticles into passive microfluidic structures using a molding technique that employed a reaction chamber. In this procedure, fluid microchannels and chamber structures were fabricated inside the PDMS using standard soft-lithography. The magnetic nanocomposite polymer was prepared by dispersing the magnetic powder into the PDMS polymer matrix with a weight percentage of 80

wt%. To fabricate directly into the chamber, the chamber was first filled with PEG. It was immediately covered and cooled, to solidify for ten minutes. Afterward, microneedles were inserted, and the composite polymer was then poured over the microneedles, while the needles were slowly pulled out. The vacuum created then drew the composite into the needle holes. Note that creating a vacuum is simply one type of degassing procedure, and other strategies can be utilized to fill the microchannels with the PDMS-magnetic mixture [7]. Continuing with the method outlined by Rahbar *et al.* [16], one reason this method is so widely used is because of its ability to produce microstructures with such high aspect ratios, up to 8:0.13. Additionally, while this method has a relatively easy procedure and is low cost, another benefit lies in that it creates very responsive films that can be actuated using *small* and *localized* magnetic fields, approximately 7 mT, whereas several other methods require a stronger electromagnet for curing. Thus, the combination of the factors listed above makes this fabrication method preferable for high volume and large scale productions of soft, magnetic films.

This molding process, which solved the issue of air bubbling through degassing techniques, has been reproduced by the likes of Khaderi *et al.* [27], Chen *et al.* [13], and Huang *et al.* [14]. However, this process does not always need to use a reaction chamber with a polymer mold that is not PDMS. Tsumori *et al.* [8] also illustrated a fabrication process similar to that of Rahbar *et al.* [16] and Chen *et al.* [11], but in this case, in a PDMS mold with cylindrical cavities, rather than a chamber with manually created needle holes. In addition, to automate the process outlined by Rahbar *et al.* [16], an alternative to filling the chamber cavities to create microchannels is by using a micro-drilling technique, highlighted by Chen *et al.* [9] [12] [46], which achieves more efficient micromixing. An advantage of this mixing, and by extension, the process as a whole, is that less beating area is required; this provides a larger degree of control

over the flow. As a result, this method is most useful for applications requiring a high density of compact design where flow must be tightly manipulated.

Another common fabrication technique, used by Belardi *et al.* [47], Fahrni *et al.* [48], and Hanasoge *et al.* [49] [50], is a subtype of stereolithography, known as two-color lithography process, where a mixed solution of a copolymer and the magnetic nanoparticles was processed by photolithography and sacrificial layer etching. In this process, Belardi *et al.* [47] described how the surface of a silicon wafer was first modified with an organosilane, before depositing a hydrophilic polymer. When exposed to ultraviolet radiation, the hydrophilic polymer underwent crosslinking to form a hydrogel, turning the surface hydrophilic. A second polymer layer, deposited by spin-coating and containing a different cross linker sensitive to radiation below wavelengths of 300 nm, anchored the structures together and acted as a sacrificial layer in the release process [48]. Then, irradiation through a structured mask anchored the polymer into strips, while the unexposed parts remained soluble. Following that, a layer of the magnetic composite was deposited and structured using ultraviolet light of wavelength 365 nm. A layer of hydrophilic polymer without photoreactive groups was then deposited on top of the developed structures by spray coating. The exposure of 365 nm radiation activated residual methacryloyloxy benzophenone (MABP) groups in the structures, thereby immobilizing a thin layer of the hydrophilic polymer. Finally, the hydrophilic polymer in the sample dissolved, along with the soluble composite behind the mask, thereby selectively etching the said sacrificial layer, as noted by Hanasoge *et al.* in two separate experiments [49] [50]. This method produces freestanding ferromagnetic composite films which can then be actuated by an external magnetic field in a number of ways.

Magnetic cilia and films can also be fabricated using many other methods. One such method is the roll-pulling process. Wang *et al.* [51] illustrated it as a process in which a cylinder decorated with micropillars was rolled over a liquid precursor film containing magnetic particles, while a magnetic field was applied simultaneously above and below the moving parts. In this method, a PDMS sheet with micropillars was attached to the surface of an aluminum roll after plasma treatment, and a layer of the magnetic precursor liquid was applied on a glass substrate. As the substrate traveled under the rotating roll, the micropillars touched the precursor liquid film, pulling out thin filaments until they reached a critical length and were removed for curing into desired structures. One of the advantages of this method is its speed; fabrication can occur up to 1 m/s, however, this can vary as it is constrained by the speed limit of the substrate. Coupled with a large production area, this high fabrication speed would be especially cost-effective for larger scale industry applications, should the substrate be replaced with one that has higher speed capabilities. Additionally, it was found that the structures produced using this method can be deformed in both 3D rotational motion as well as 2D planar motion, making it an ideal method when focusing on the flexibility of films. Furthermore, it was determined that increasing the PDMS content resulted in a higher yield stress and also retention of more of the filament lengths during the extraction portion of the process. Thus, for the fabrication of soft, magnetic films as discussed in this paper, this method becomes more favorable as the PDMS content increases; it would increase the maximum stress that the film could experience without causing plastic deformation.

VII. B. ii. Additively Fabricated Soft, Magnetic Thin Films

Additive manufacturing methods have been extensively used for fabricating soft, magnetic films, structures, and devices. Additive manufacturing has evolved as an emerging and

popular method for fabricating magnetizable microstructures by adding material layer by layer to create a complete structure. The first light-based subset of additive manufacturing methods include stereolithography (SLA), digital light processing (DLP), and direct laser writing (DLW), all requiring photosensitive resins in order to cure liquids into a solid to produce a 3D printed component or trace. For all of these cases, liquid ink baths are irradiated with different wavelengths of light (e.g.., lasers in SLA and DLW and projectors in DLP) [52]. Due to the extent of control achievable by varying the magnitude of the incident radiation, these methods are able to produce 3D-printed components and devices with very high resolutions. On the other hand, photosensitive resins are generally brittle and require complex formulations to achieve photocurability. Photosensitive chemicals used in resins are also typically cytotoxic leading to low biocompatibility for biomedical applications. Developing biocompatible photosensitive resins is an active field of research. Additionally, there is a lack of published research on soft photosensitive resins, which are commercially available.

Another subset of common methods involves binding solids together, such as fused deposition modeling (FDM), direct ink writing (DIW), and binder jetting. FDM is the most commercially popular method of 3D printing due to its speed, scalability, and safety. However, the details/resolutions of the features of the printed components that the FDM process is capable of achieving is often very low [52]. DIW and binder jetting, on the other hand, are more complex and less common than FDM. DIW requires shear-thinning inks for printing, severely limiting the available printing options, but allowing for increased resolution. Binder jetting deposits layers of polymer powder onto the print stage and uses a laser or a liquid binder to build layers of polymer together, in a way that is very similar in concept to direct metal laser sintering.

FDM has emerged as an important method to 3D print soft magnetic materials and films. For example, Qi *et al.* [20] fabricated a soft magnetic material by employing FDM that considered a rigid magnetic filament fabricated using a mixture of NdFeB nanoparticles and PLA. The resulting magnetic filament was magnetized during the extrusion process in order to align the magnetic particles to achieve anisotropic magnetic properties. This approach was limited by the minimum print precision of their FDM printer at 0.1 mm, restricting their structures to large-scale sizes [20]. Ji *et al.* 3D-printed a semi-flexible soft magnetic actuator by employing DLP [35]. The materials used consisted of a polyethylene glycol based resin embedded with Fe_3O_4 NPs with a mean NP diameter of about 200 nm, and showed the effect of weight percent on mechanical properties.

Alternative manufacturing processes include using 3D printing to create molds for soft magnetic materials. In research done by Iacovacci *et al.* [53], molds were created using 3D-printing, which were then used to cast soft magnetically actuated components used for robotic applications. To align and magnetize the NdFeB particles, a 3T MRI scanner was aligned with the static magnetic field directed in the same direction as the robot axis.

Other fabrication methods have also been used to create rigid magnetic structures. Li *et al.* [54] used photo-lithography to build complex robotic shapes designed to carry cells to application sites. SU-8 was used as the base resin for laser lithography to achieve a complex geometric shape. The resin was subsequently coated with Ni and Ti to achieve magnetic properties and biocompatibility respectively. Similarly, Huang *et al.* [55] used a combination of 3D direct laser writing and selective physical vapor deposition to manufacture a biocompatible magnetically controlled robot that can deliver material such as drugs to specific application sites.

Uniquely, this fabrication method allows the use of a complex mechanical delivery mechanism based on an Archimedes' screw (see Fig. 2 (a)). The structural base was manufactured using 3D laser lithography on SU-8 resin over a silicon dioxide substrate. This component was then covered in Ni and Ti using vapor deposition. Another study [44] also used 3D laser lithography to create a structure out of SU-8 resin on top of a glass substrate, before applying a biocompatible Ni and Ti coating to impart magnetic properties. The resulting magnetically controlled robot can be used to culture cells and maneuvered towards application sites (see Fig. 4 (b)).

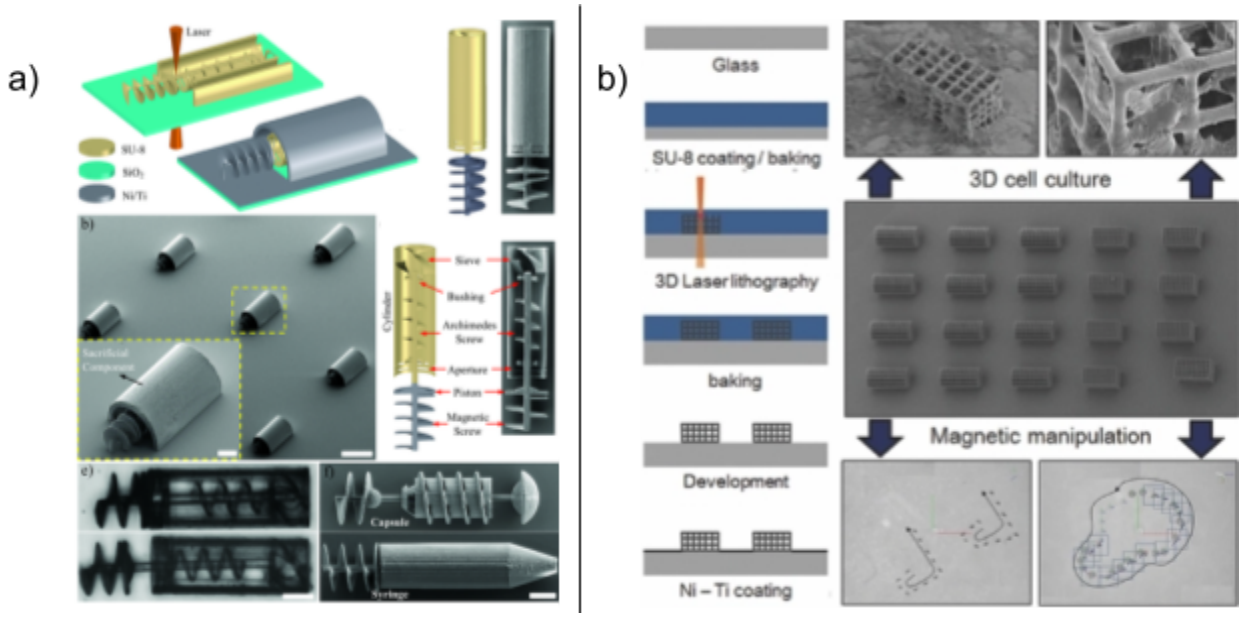

Figure 3. Examples of magnetically controlled robots fabricated using additive manufacturing processes. (a) Example of a magnetically controlled robot that uses an Archimedes' screw to deliver drugs to applications sites, reproduced from [55]. (b) An example of a magnetically controlled robot carrying cell cultures to application sites, reproduced from [44].

VII. C. Characterization

In this section, we will discuss the mechanical and magnetic properties of physically soft, magnetic films and how to evaluate or quantify those properties.

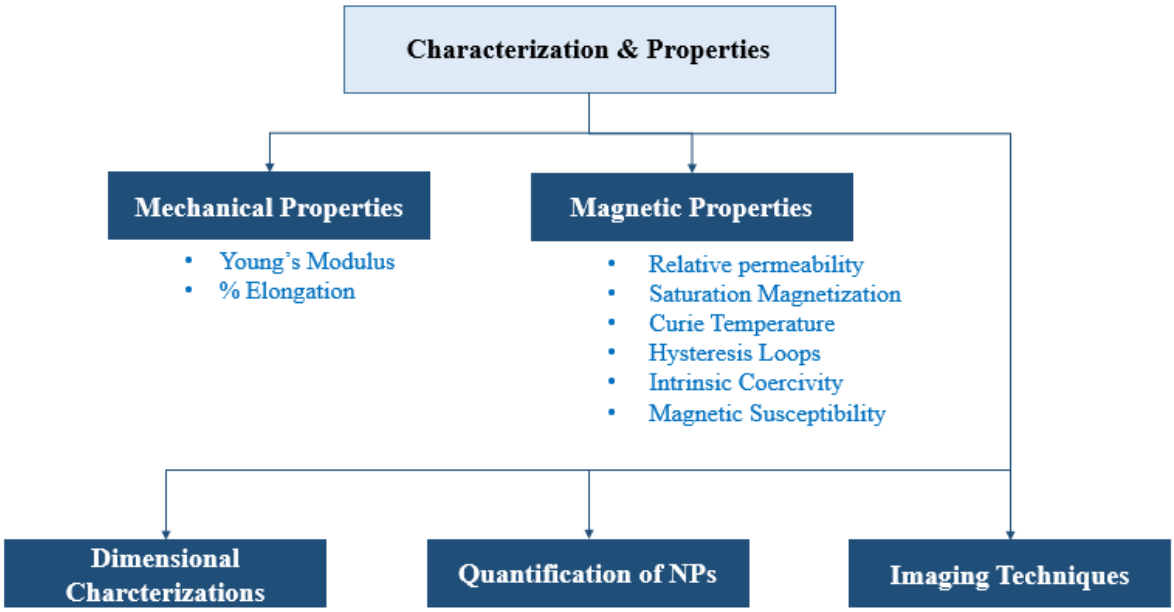

Figure 4. Schematic describing an overview of the different characterizations of the thin magnetic films and the properties exhibited by them. In this section, the mechanical and magnetic properties are discussed, followed by the dimensional characterizations in terms of film thickness, the quantification of nanoparticle sizes and the imaging techniques employed for quantifying each of them.

VII. C. i. Mechanical Characteristics and Properties

Owing to the flexible and compliant-nature of the physically soft, magnetic films, the mechanical properties can be characterized by their elastic modulus (i.e. Young's modulus), concentration of microparticles or nanoparticles, shear modulus, and fracture strain.

The elastic modulus is a key property of these films. Table 4 shows the calculated Young's modulus values of different magnetic films from the experiments outlined by Wang *et al.* [1]. These values indicate that films consisting of PDMS with larger elongation have smaller Young's modulus (and hence are less stiff) as compared to the films consisting of PDMS with smaller elongation. These values also indicate that the film thickness has no bearing on Young's modulus values and that the films with small ferrite powders have smaller Young's modulus values. Due to the low tensile strength of these films, permanent deformation due to yielding can be a concern, especially in biomedical applications where precision is of the utmost importance [56].

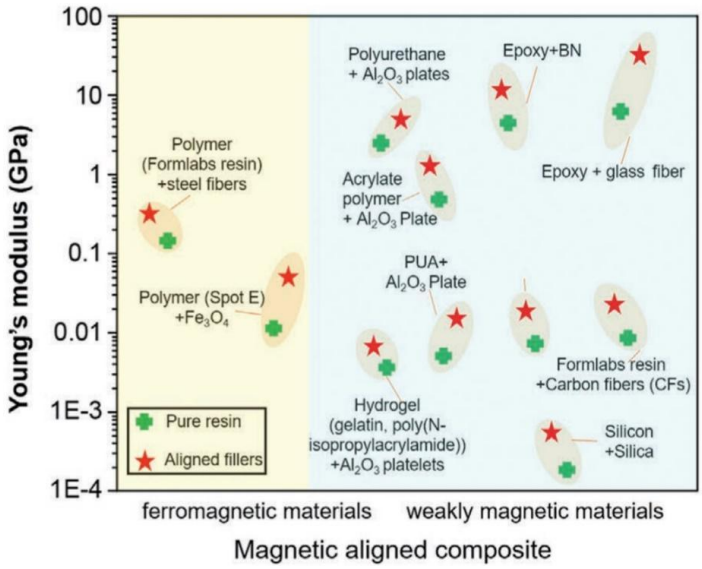

Figure 5. Plot showing the range of Young's modulus values of various ferromagnetic and weakly magnetic materials embedded in different polymer matrices [18]. The figure has been reproduced with permission from C. Zhang *et al.*, "3D Printing of Functional Magnetic Materials: From Design to Applications," *Advanced Functional Materials*, vol. 31, no. 34, pp. 2102777, 2021, doi: 10.1002/adfm.202102777. Copyright (2021) WILEY‐VCH Verlag GmbH & Co. KGaA,

PDMS	Magnetic powders	PDMS:powder ratio (by weight)	PDMS elongation (%)	Thickness (µm)	Young's Modulus (MPa)
186	none	Pure PDMS	420	62	1.576
3-1753	none	Pure PDMS	120	35	1.970
186	NdFeB	1:1	420	82	2.260
3-1753	Hard ferrite	1:1	120	40	9.906
3-1753	Hard ferrite	1:1	120	69	9.996
3-1753	NdFeB (grinded)	1:1	120	61	13.40
3-1753	NdFeB	1:1	120	126	16.60
3-1753	NdFeB	1:1	120	216	17.10
3-1753	NdFeB	1:4	120	128	28.90

Table 4. Calculated Young's Modulus values from the experiment conducted by Wang *et al.* [1]. The table has been reproduced from [1] with permission.

The elastic modulus can be evaluated through the use of a tensile testing machine (e.g. MTS Nano Biomix, Agilent Systems) [21]**,** or through thermo-mechanical methods (e.g. TMA 2940-Q series, TA Instruments) [5]. In both the cases, uniformly sized samples of the film are cut and then clamped at two ends. Forces are slowly applied to the sample and the resulting strains are measured either by directly measuring deformation (for the case tensile testing method) or by employing a thermocouple (for the case of thermo-mechanical method). For samples whose

dimensions are in the range of 10μm - 1000μm, the latter method is found to be easier to perform.

If the MNPs are sufficiently small as compared to the film dimension and are uniformly dispersed throughout the film, the magnetic film can be considered to be homogeneous and isotropic. For this case, the following simple relationship can be used to determine the film's twistability:

$$E = 2G(1 + \nu) \quad (1)$$

If the magnetic domains of the film are organized, the film could exhibit anisotropy, especially so when magnetized. The above relationship will not hold in such a case. In [22], higher shear moduli were observed in a film that was fabricated in presence of a strong external magnet used to orient the MNPs.

The concentration and particle size of MNPs is a key factor in determining the macro-characteristics of the soft, magnetic film. These parameters are almost always known and intentionally varied to produce a film with the desired properties. For example, for the case of a PDMS polymeric matrix, when one varies the concentrations of the ferrite particles, a positive correlation between the weight percentage of the ferrite particles and the modulus of elasticity is obtained [1], [4]. SEM or TEM is often used to observe the distribution and size of the MNPs (such as the ferrite particles) throughout the film [4], [5], [21], [22].

VII. C. ii. Magnetic Characteristics and Properties

The magnetic properties of these films include their relative permeability μ_r, saturation magnetization H_s (or saturation induction B_s), intrinsic coercivity H_c, curie temperature T_c, hysteresis loops (M-H). These properties will vary depending on the type of the MNPs used and

the concentration (and size distribution) of the MNPs in the polymeric matrix. Saturation magnetization refers to the state of a material when its magnetization has reached a maximum value, whereas intrinsic coercivity refers to the magnetic field required to demagnetize the material. Since soft magnets (i.e., magnets with soft magnetization properties) can be easily magnetized and demagnetized, they exhibit high relative permeability, high saturation magnetization and low coercivity, whereas hard magnets (i.e., magnets with hard magnetization properties) show the opposite behavior. Curie temperature refers to the temperature beyond which a magnet loses its magnetic properties. Hysteresis loops are crucial in determining a magnet's properties and subsequent applications. Soft magnets (magnets with soft magnetization properties) exhibit low hysteresis losses whereas hard magnets (magnets with hard magnetization properties) exhibit larger hysteresis losses. Other important magnetic properties are coercive force withstandability and magnetic susceptibility. Coercive field withstandability refers to the ability of a material to withstand an external magnetic field without demagnetizing [56]. Susceptibility dictates how much the film will magnetize for some applied magnetic field. Larger values of susceptibility for a magnetic nanocomposite ink will imply that the ink will be more reactive to the presence of a magnetic field, which allows a greater range of motion for the film or cilia given the same magnet and material elasticity [7], [16].

These properties can be measured using a vibration sampling magnetometer [17], [23] or microscopic imaging [57]. First, methods of quantifying magnetic saturation must be discussed. Novakova *et al.* [58] performed experiments with three different magnetic field directions when measuring magnetic saturation: along the film plane and perpendicular to the film plane. The data clearly showed that while the magnetization lay in the film plane, it also had a preferable

direction, indicating a lamellar arrangement of particles within the film [58]. The lamellar structure is found out by analyzing the magnetic anisotropy (SIRM and NRM) vectors.

Additionally, while conversion electron Mossbauer spectroscopy was also performed by Bando *et al.* [59] to measure anisotropy in the film plane, it was in the study of Novakova *et al.* [58] that the spectra from the subsurface regions of the film demonstrated superparamagnetic doublets, confirming high anisotropy as a result of non-homogenous distribution of nanoparticles within the film interior. The study [58] concluded that the strongly interacting magnetic particles that produce strong saturation magnetization are located in the middle of the film, forming a lamellar structure. This, along with the data from the study of Bando *et al.* [59] that showed that coercive force withstandability and the magnetic saturation increased with the substrate temperature, helped to infer that larger grains within the bulk of thicker films led to an increase in magnetic saturation and coercive force withstandability. With a higher value of magnetic saturation, the film can act as a stronger magnet, which when coupled to a higher coercive force withstandability made the film less likely to become demagnetized.

Finally, the magnetic properties of NdFeB inks (NdFeB particles are magnetic particles with hard magnetic properties) were found to be linearly dependent on the percentage (with respect to the background polymeric matrix) of magnetic particles included: a higher ratio of NdFeB to PDMS led to higher values of all the magnetic properties mentioned above [15], [22].

VII. C. iii. Dimensional Characterizations

A large subgroup of the films under consideration are in the form of cilia or cilia-like structures. Cilia are characterized by their high aspect ratio and smaller cross section. They can vary in pillar diameter to as small as 200 nm [60], though typically their widths are in the range

of 1-50 μm [7], [16], [61]–[63]. Limits on aspect ratio are governed by the strength of the applied magnetic field. Rahbar *et al.* [16] found that for lengths greater than 1 mm, cilia in an array tend to bend toward each other (or might actually collapse) if spaced less than 500 μm apart. A common characteristic of cilia is that they tend to be anisotropic; different properties (e.g. magnetic susceptibility, Young's modulus) are different along different layers or axes of the structure [27].

The thickness of magnetic films is crucial in determining the variation of magnetic properties. In their experiments, Ariake *et al.* [64] experimented with FeCo-Al thin soft magnetic films whose dimensions were in the range of 11nm - 120nm. All M-H hysteresis curves exhibited high squareness, and equal amounts of saturation magnetization. The coercivity was smallest for the 11-nm thin film; the coercivity first increased (up to a film thickness value of 50 nm) and then decreased with the film thickness [65]. This behavior can be attributed to the magnetoelastic effect, i.e., stress induced magnetic anisotropy [64]. Also, it was found that these properties do not vary linearly with the film thickness.

VII. C. iv. Quantification of Nanoparticle sizes

When quantifying nanoparticle sizes, parameters such as crystallite size, particle size, and particle shape are all to be considered. Crystallite size can be determined via X-ray diffraction (XRD). By measuring the peak broadening and utilizing the Scherrer equation, crystallite size (limited to around 100 nm) can be quantified. In addition to the crystallite size, the actual particle size can be determined via other optical methods. Dynamic light scattering (DLS) can be used to determine the nanoparticle size distributions. In combination, XRD and DLS can be used to estimate the crystallinity of NPs which can affect their magnetic domains and properties. These

methods largely assume spherical NPs. Small Angle X-ray Scattering can also be used to determine the particle shape by comparing the measured intensity of the scattered x-rays to the wavenumber of incident light.

VII. C. v. Imaging Techniques

Direct imaging can greatly assist the characterization of a film. Scanning electron microscopy (SEM) is commonly used to determine nanoparticle agglomeration [4], and other structural and morphological properties [20], [32], [37]. In addition to SEM, other common microscopy techniques, such as transmission electron microscopy (TEM) and fluorescence microscopy, are used to directly confirm or detect microstructures [9], [12], [15], [19], [35], [41], [44]. X-ray diffraction is also occasionally used to detect crystalline portions in the polymer [35], [44].

The dimensional quantification of the soft, magnetic film is highly relevant. Film thickness, for example, is commonly measured through both scanning probe and optical microscopy. Scanning probe methods for thin film thickness include Atomic Force Microscopy (AFM). Optical methods include ellipsometry, where the polarization of incident and scattered light is compared for determining the optical properties (of the film) like refractive index, in addition to determining the film thickness.

VIII. Methodology

VIII. A. Materials

The materials used in our composites can be largely divided into two categories. Like many composites, new materials are synthesized with the intent of selecting ideal properties from the individual materials to create new materials with unique properties. For example, carbon fiber reinforced polymers (CFRP) consist of two materials: a polymer matrix and carbon fibers. The polymer matrix provides rigidity while the carbon fiber provides high tensile strength creating an extremely lightweight and strong material.

For our physically soft magnetic films, there are two components that give rise to the mechanical and magnetic properties observed, a PDMS polymer matrix and Fe_3O_4 NPs. The PDMS acts as a physically soft and mechanically compliant film as described in the above sections while the Fe_3O_4 provides the film's magnetic properties. In addition to these materials, xylene was used to prevent the aggregation of Fe_3O_4 NPs, a phenomenon documented in NPs [18]. The modification with xylene also prevents the oxidation of the Fe_3O_4NPs.

VIII. B. Experimental Methodology

To prepare the magnetic particles, the Fe_3O_4 NPs between 20-30 nm were combined in oleic acid and stirred at 60-80 ℃. The oleic acid coating helps prevent oxidation of the Fe_3O_4 NPs and reduces surface tension between the NPs and polymer matrix by acting as a surfactant. To prepare the polymer matrix, PDMS-A was mixed with an isomeric mixture of ortho, para, and meta xylene and stirred at room temperature. The xylenes help reduce the density of the PDMS.

The Fe_3O_4-oleic acid and PDMS-xylene mixtures were combined and ultrasonicated for 12 hours. PDMS-B, the curing agent, was then added to the mixture. The mixture was subjected to a vacuum treatment to remove trapped air and set to cure at room temperature for 24 hours or at 120 ℃ for 12 hours. No meaningful difference in magnetic properties was observed for the two curing procedures. The cured films were then cut to uniform size. These films, in undeformed, folded, and twisted configurations, were then magnetically characterized using a Lakeshore Vibrating Sample Magnetometer.

IX. Results & Discussion

IX. A. Hysteresis Curves and Data Collection

A total of 6 sample films underwent magnetization testing. These samples represent two different concentrations of Fe_3O_4 particles. The first is a low iron oxide concentration, with the ratio of PDMS to Xylene to Iron Oxide being 1:1:0.5. The second is a high iron oxide concentration, with the ratio of PDMS to Xylene to Iron Oxide being 1:1:1. Both sets of samples were tested in undeformed, folded, and twisted orientations. The films with high iron concentrations were additionally tested in an out-of-plane orientation.

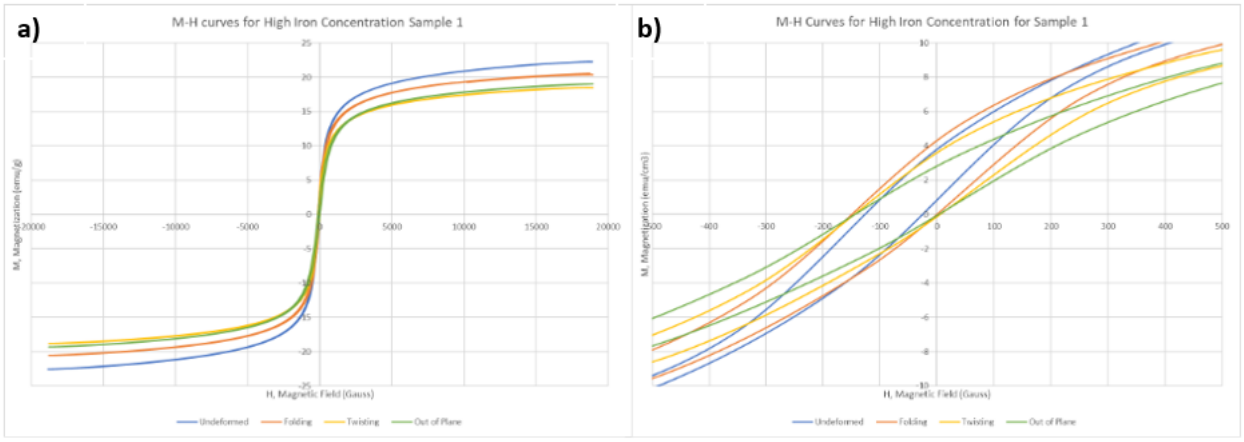

Figure 6. M-H curves of sample 1 of the high iron concentration film, demonstrating hysteresis, both (a) and (b) show the same data, with (b) being focused on the origin. The asymptotic peak of part (a) represents the magnetic moment or saturation magnetization. The y-intercept of (b) represents latent magnetization. The x-intercept of (b) represents the coercivity.

The resulting M-H curve for sample 1 of the high iron concentration films can be seen in Figure 6. This figure is representative of the M-H curves of all other samples. From this figure, the coercivity, latent magnetization, and magnetic moment or saturation magnetization were

recorded. These measurements can be seen in Tables 5-7. As a note, magnetization measurements were recorded on a per weight (per gram) basis instead of a per volume (per cm^3 basis (as preferred in the literature), due to irregularities in the samples making accurate volume measurements difficult to obtain.

Table 5. Saturation Magnetizations of different samples of magnetic films with both low and high iron oxide concentration orientations for different film orientations.

Saturation Magnetization (emu/g)	Undeformed	Folded	Twisted	Out of Plane
Low Iron Concentration				
Sample 1	18.27	23.58	16.60	x
Sample 2	7.33	7.84	7.84	x
Sample 3	8.11	8.48	10.97	x
Average	11.24	13.56	10.97	x
High Iron Concentration				
Sample 1	22.26	20.52	18.53	18.99
Sample 2	20.73	17.52	20.73	14.72
Sample 3	18.00	25.22	22.86	19.64
Average	20.33	21.09	20.71	17.78

Table 6. Latent Magnetizations of different samples of magnetic films with both low and high iron oxide concentration orientations for different film orientations.

Latent Magnetization (emu/g)	Undeformed	Folded	Twisted	Out of Plane
Low Iron Concentration				
Sample 1	4.04	5.03	3.32	x
Sample 2	1.64	1.70	1.36	x
Sample 3	1.76	1.78	1.61	x
Average	2.48	2.83	2.09	x
High Iron Concentration				
Sample 1	3.72	4.10	4.42	2.74
Sample 2	3.41	3.32	3.60	1.87
Sample 3	2.96	4.91	4.16	2.79
Average	3.36	4.11	4.06	2.47

Table 7. Coercivity of different samples of magnetic films with both low and high iron oxide concentrations for different film orientations.

Coercivity Magnetization (G/g)	Undeformed	Folded	Twisted	Out of Plane
Low Iron Concentration				
Sample 1	4712.5	4577.2	4385.1	x
Sample 2	8025.3	6839.8	4809.9	x
Sample 3	3952.8	3712.9	3553.7	x
Average	5300.9	4842.0	4169.5	x
High Iron Concentration				
Sample 1	2766.1	3309.56	3198.1	3188.6
Sample 2	4016.7	4636.5	4719.7	4326.7
Sample 3	3837.3	4797.5	4660.5	4626.3
Average	3432.4	4117.8	4054.6	3928.3

IX. B. Saturation Magnetization Results

Figure 7 shows the comparative performance of magnetization for samples in different orientations. From this information, we can see that there is no significant difference between the saturation magnetizations of the films in different orientations, either during in versus out of plane undeformed samples (paired T-test P-value of 0.8935), low iron concentration samples in different orientations (one-way ANOVA P-value of 0.9286), or high iron concentrations (one-way ANOVA P-value of 0.949).

However, there is a comparative difference between the saturation magnetization of the low iron and high iron concentration samples. The high iron concentration samples are statistically greater than those of the low iron concentration samples (T-test P-value of 0.003374).

Our saturation magnetization values are difficult to compare to those of other magnetizable films produced in the literature. This is because of the unique nature of our films where nano-scale soft magnetic particles are suspended within a PDMS matrix instead of being contained with a separate layer. However, with this caveat understood, our saturation magnetization values are within the same order of magnitude as other reports of soft magnetizable films [66]–[69].

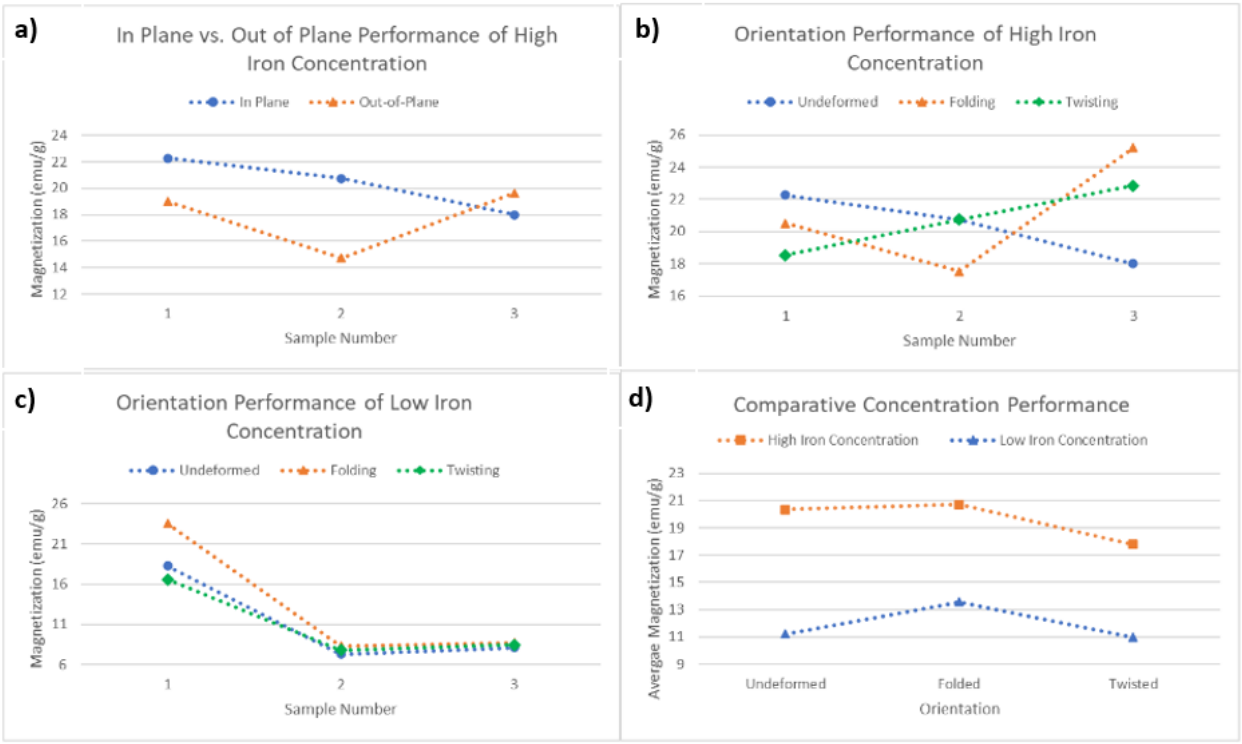

Figure 7. Magnetization results of samples. (a) demonstrates the in-plane versus out of plane performance of high concentration iron. (b) demonstrates the performance of high iron concentration films in different orientations. (c) demonstrates the performance of low iron concentration films in different orientations. (d) demonstrates the comparative average performance of low and high iron concentration films across different orientations.

IX. C. Latent Magnetization Results

Figure 8 shows the comparative performance of samples of a single concentration in different orientations. From this information, we can see that there is no significant difference between the saturation magnetizations of the films in different orientations, either during in versus out of plane undeformed samples (paired T-test P-value of 0.1528), low iron concentration

samples in different orientations (one-way ANOVA P-value of 0.8338), or high iron concentrations (one-way ANOVA P-value of 0.2695).

However, there is a comparative difference between the latent magnetization of the low iron and high iron concentration samples. The high iron concentration samples are statistically greater than those of the low iron concentration samples (T-test P-value of 0.01192).

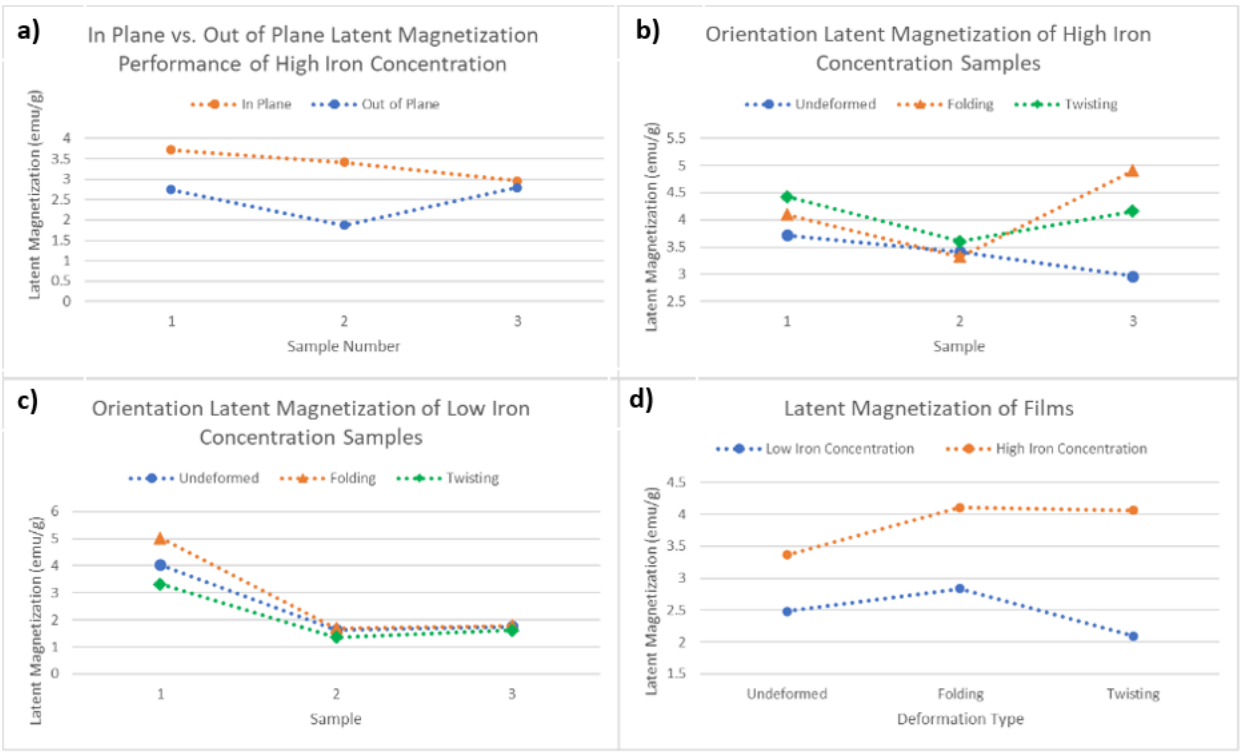

Figure 8. Latent magnetization results of samples. (a) demonstrates the in-plane versus out of plane latent magnetization of high concentration iron. (b) demonstrates the latent magnetization of high iron concentration films in different orientations. (c) demonstrates the latent magnetization of low iron concentration films in different orientations. (d) demonstrates the comparative average latent magnetization of low and high iron concentration films across different orientations.

IX. D. Coercivity Results

Figure 9 shows the comparative performance of coercivity for samples of a single concentration in different orientations. From this information, we can see that there is no significant difference between the saturation magnetizations of the films in different orientations, either during in versus out of plane undeformed samples (paired T-test P-value of 0.7776), low iron concentration samples in different orientations (one-way ANOVA P-value of 0.6236), or high iron concentrations (one-way ANOVA P-value of 0.5131).

However, there is a comparative difference between the coercivity of the low iron and high iron concentration samples. The high iron concentration samples are statistically greater than those of the low iron concentration samples (T-test P-value of .001833).

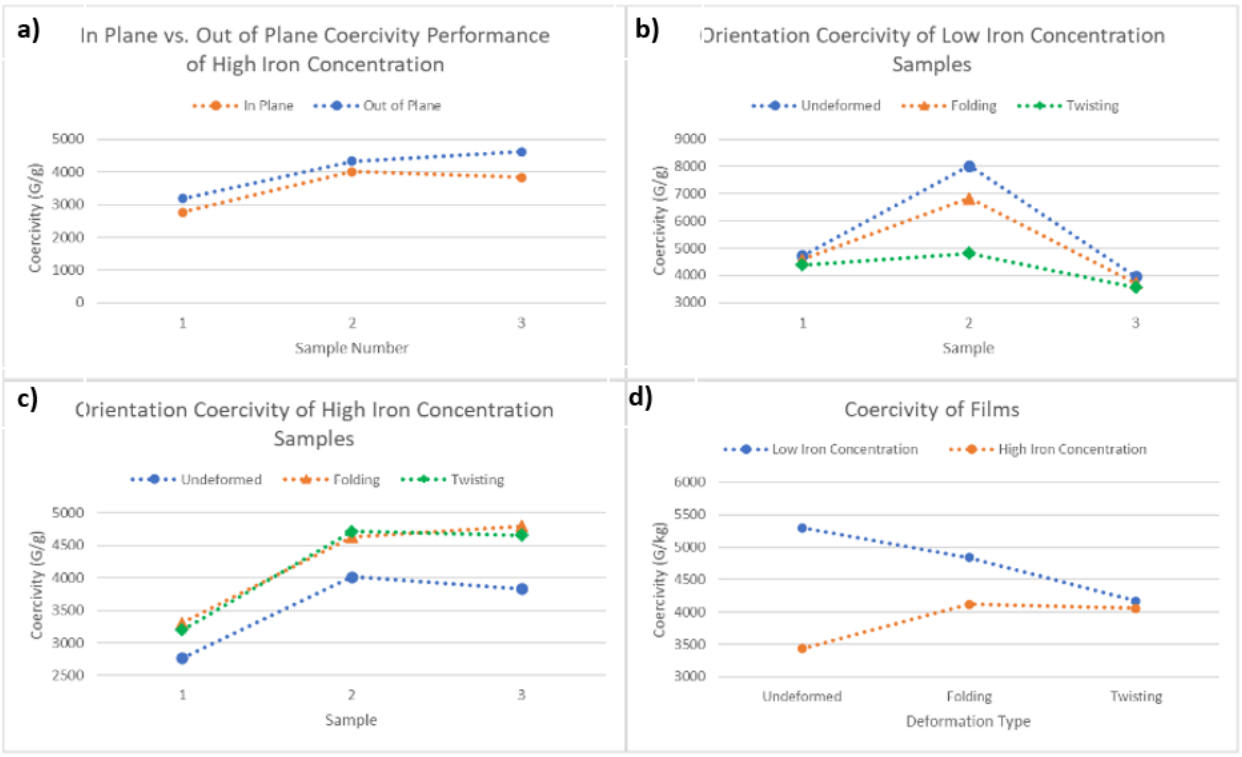

Figure 9. Coercivity results of samples. (a) demonstrates the in-plane versus out of plane

coercivity of high concentration iron. (b) demonstrates the coercivity of high iron concentration films in different orientations. (c) demonstrates the coercivity of low iron concentration films in different orientations. (d) demonstrates the comparative average coercivity of low and high iron concentration films across different orientations.

IX. E. Discussion

Our results first reveal the soft magnetic properties of these films. The initial M-H curves developed during testing demonstrate considerably narrow hysteresis curves, a sign of soft magnetic properties of our materials. Our results also reveal that there is a correlation between a higher concentration of Iron Oxide nanoparticles within our films and increased saturation magnetization and latent magnetization as well as decreased coercivity. The presence of these particles directly impacts the magnetic capability of these films. These films also demonstrated a saturation magnetization in the range of 7-26 emu/g. While this method of suspending nanoparticles within a matrix of PDMS is novel, these values are comparable with other methods of soft magnetic film production, such as layering magnetic and non-magnetic particles and the use of larger magnetic particles. These results therefore show that our relatively simple manufacturing process for these demonstratively effective materials is a valid new avenue of magnetic film production.

These results also demonstrate that this ink composition and manufacturing process are able to produce magnetizable films that are able to maintain a flexible structure that allows for bending and twisting. The saturation magnetization values for our films did not change significantly when undergoing extreme deformation such as bending, twisting, or being turned

out of plane. These films are therefore highly robust, allowing for an increased potential capability of this material in future use and applications.

As our sample sizes for this initial exploration are considerably small, larger scale testing of this same concept is recommended to confirm these results. Additionally, an interesting further avenue of study would be to test whether the successive testing of these films is affected by the film's first test. In our testing procedure, each sample was tested first in the undeformed state, then folded, then twisted, etc. Future work should vary the first test completed on a particular film within a single batch of ink in order to determine if the original testing in any way affects our later measurements.

Ultimately, from this initial exploratory testing it is clear that the use of soft magnetic particles suspended within a larger matrix is an exciting new avenue for the development of soft magnetic materials, particularly robust magnetic materials and films. There is clear evidence that our relatively simple manufacturing process could be used as a part of the future of research into these materials.

X. Global Equity Analysis

Accessible information is understood to cover all information that is provided in such a form that allows every user and individual to access content on an equal basis with others [70]. It encompasses knowledge that individuals can easily orient themselves to, and that can be understood by different cognitive styles, such as eyesight, hearing, and fingers/touch [71]. As researchers, it is our job to utilize technology to create and share information with not only the scientific community, but also the broader public as a whole, in order to promote a culture of inclusivity and progress.

One of the greatest global equity issues is accessibility. Most notably, accessibility to information, which over time, has created a largely unequal distribution of knowledge amongst a few, compared to the masses. This particular issue is very prevalent in the research community. Many research outputs and experimental findings are hidden behind paywalls or require premium access to specific journals through institutional logins, thus making research more difficult to be held accountable to the public [72]. Additionally, this limited dissemination of information restricts the ability to compile knowledge together in a single platform [72]. With the sheer amount of research that is produced day by day, it can be arduous and cumbersome for individuals to sort through and find the information they need, whether that is for personal reasons or professional responsibilities.

Our Gemstone team spent the past four years trying to bridge this gap in knowledge availability, and level the unequal distribution in access. Our impact on global equity is focused on writing and publishing a review article that consolidates major information on these soft, thin, composite films and their applications. Since this area of research is very niche and specialized

in a small subset of the larger materials science community, we focused our efforts on summarizing as much information as possible on the properties, fabrication techniques, characterization, and large-scale applications of said films. It was done this way so that other researchers and individuals would not have to scrounge for information they need, and could find a majority of it in a localized place. Furthermore, the team specifically chose to submit the article to a well-known peer-reviewed journal, because of their wide, global audience online and so that we may reach as many individuals as possible.

Another equity goal that the team achieved was to write the article in such a language that is easier to digest and understand by masses. Many articles with promising information are often left unread and uncited by students and younger, inexperienced researchers due to the difficult language, high-level vocabulary, or presence of graphs/visuals that are hard to decipher. It is an issue that the team has experienced not only personally, but that they have witnessed amongst peers at the university and professional settings. As a result, the diction of the team's review article was carefully developed so that larger audiences could better comprehend the scientific concepts behind these films, with the minimal requirement that said readers have some basis of scientific knowledge in this area. Furthermore, the team designed their own graphics to supplement the article, styled intentionally simplistic, to help guide the reader throughout the summary of these films, and to further assist those who learn through more visual perception channels.

Coupled with the ease of access to information, the team's experimental design was constructed to keep in mind accessibility to raw materials. Team GECKO's research chose PDMS as the base polymer in these soft, composite films, due to the nature of its good thermal stability, gas permeability, easily modifiable properties, and how commercially available it is to

acquire from global distributors like Dow Corning and Sigma-Aldrich [73]. Furthermore, what makes PDMS a more commonly used and readily available material is that it is inexpensive compared to other polymeric substances. PDMS costs approximately half the price of polyurethane ($0.07/g vs. $0.15/g) and about 1/15 of the price to purchase a gram of SU-8 photoresist; and since it does not require a development step to remove excess, unexposed photoresist, it is also associated with lower operating costs in the overall manufacturing process [74].

Overall, the team emphasized accessibility to information and raw materials in their research efforts to promote global equity. Be that as it may, the team hopes to continue these equitable endeavors in the future, and expand upon them through more in-depth research analysis.

XI. Conclusion

XI. A. Applications

The contents of this section have been published in the Journal of Materials Chemistry C in a paper written by the authors of this work.

Devices and objects, several of which are inspired by the structures in microorganisms (see Figure 10), fabricated or printed with soft, magnetic inks have been employed for several applications. In this section, we summarize some of these applications.

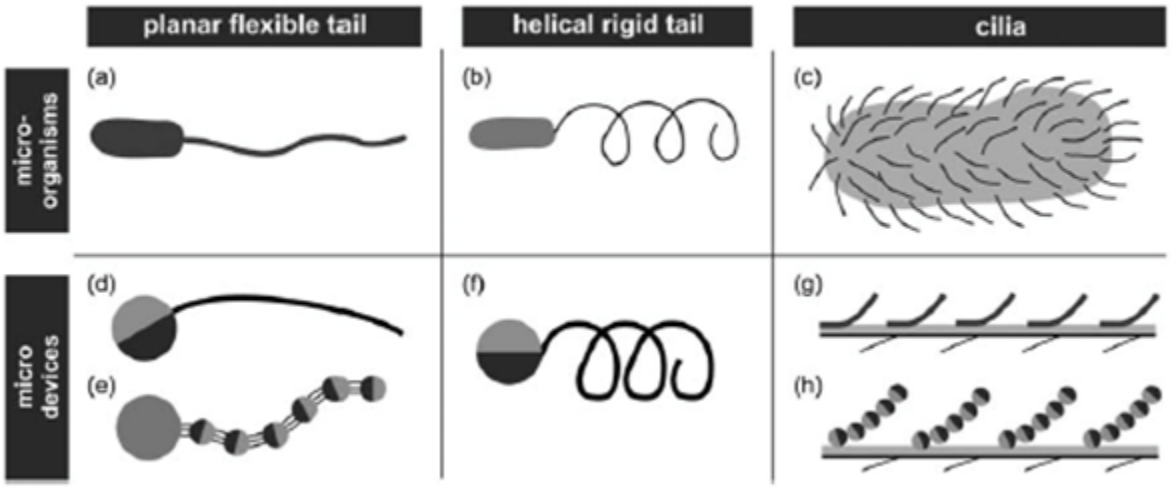

Figure 10. Schematic depicting motion-inducing structures in microorganisms and the corresponding biomimetic elasto-magnetic microdevices. (a) Flexible planar flagella of microorganisms like Spermatozoa. (b) Rotating helical flagella in E. coli. (c) Cilia-rich surface in microorganisms like Paramecia. Microdevices mimicking (d, e) flexible planar flagella, (f) rotating helical flagella, and (g, h) cilia [75].

The magnetic actuation of a micro/nanoscale object relies on the impartation of a magnetic torque or a magnetic force on the object by an external magnetic field. For example, the magnetic torque T_m (in N·m) that a magnetized object (with magnetization $\boldsymbol{M}$, in A/m) experiences when placed in an external magnetic field $\boldsymbol{B}$ (in T) can be expressed as:

$$T_m = V\boldsymbol{M} \times \boldsymbol{B} \tag{2}$$

where V (m^3) is the volume of the object. On the other hand, the magnetic force $\boldsymbol{F}_m$ (N) experienced by the object can be expressed as:

$$\boldsymbol{F}_m = V(\boldsymbol{M}\nabla)\boldsymbol{B} \tag{3}$$

The magnetization $\boldsymbol{M}$ depends on the magnetic nature of the object. For a permanent magnet $\boldsymbol{M}$ is a constant, while for soft magnetic, paramagnetic, and superparamagnetic objects which become magnetized only in presence of an external magnetic field $\boldsymbol{M}$ varies with the magnetic field and the shape of the object.

According to eqs. (2, 3), a magnetic object will not experience any force in a uniform magnetic field and the magnetic torque persists as long as the magnetization $\boldsymbol{M}$ does not become collinear with the magnetic field $\boldsymbol{B}$. Under such circumstances, a continuous actuation (which is required to ensure sustained propelling motions) requires the presence of a magnetic field that either has a spatial gradient or undergoes a time-dependent change (i.e., undergoes rotation, precession, oscillation, or on-off states).

The continuous actuation of the magnetic objects, often placed in a liquid medium, perturbs the surrounding liquid. This induced liquid motion is captured through the combined Navier-Stokes and continuity equations, where the effect of the motion of the magnetically

actuated objects enters through the corresponding no-slip boundary condition at the surface of the objects (i.e. the liquid velocity at the surface of the object will be identical to that of the object). In other words, the presence of these magnetically actuated objects within the liquid medium creates local velocity points within the static liquid, which lead to a net flow of liquid. Depending on the structure and arrangement of these magnetic objects and the nature of the magnetic actuation they are subjected to, the resulting hydrodynamic effects (i.e., the effects associated with the perturbation of the liquid) are capable of inducing high-velocity liquid flows in microfluidic systems [28], [63], enabling microfluidic mixing of particles and liquids [16], propelling microbots grafted with such actuatable elasto-magnetic objects [76], among other things.

XI. A. i. Actuation, Propulsion, Locomotion, and Mixing Applications

The compliance and magnetic actuatability of components and devices fabricated using soft, magnetic inks has opened the door for significant applications in small-scale actuation, propulsion, and locomotion. In most cases, such propulsion and locomotion is obtained by fabricating elasto-magnetic biomimetic structures such as cilia and flagella of different shapes that are actuated by magnetic fields to create different types of motion (see Figure 11). Recently, there has been a lot of research concerning potential means of actuation, propulsion, and mixing at the microscale. These functions are important for lab-on-a-chip systems. At the microscale, where viscous forces dominate inertial forces, traditional means of actuation, propulsion, and mixing are ineffective. Thus, efforts have been focused on developing means of actuation, propulsion, and mixing that mimic those found in nature. Researchers are using different

fabrication methods to create microrobots and artificial cilia with a wide range of dimensions for a myriad of applications.

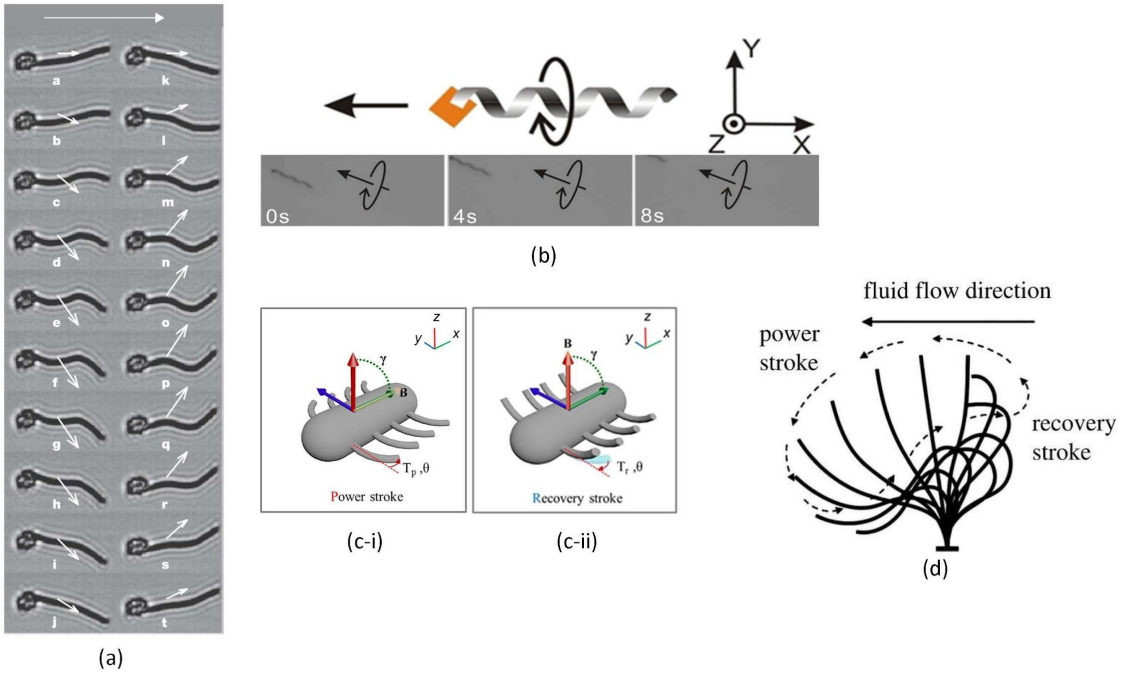

Figure 11. Microbots have been shown with the following methods of microcilia-based propulsion: (a) flexible propeller, (b) helical propeller, and (c, d) power stroke. The actual method of propulsion is displayed. (a) has been reproduced from reference [75]. (b) has been reproduced from reference [77]. (c) has been reproduced from reference [76]. (d) has been reproduced from [78].

Khaderi *et al.* fabricated magnetically-actuated cilia by embedding thin polymer films with superparamagnetic nanoparticles; the team found that the performance of these cilia arrays is similar to the performance of typical dynamic pumps indicating the potential means of mixing and transporting fluids in lab-on-a-chip systems [28]. Hussong *et al.* fabricated magnetically

actuated cilia by embedding superparamagnetic nanoparticles in a polymer matrix; with a capacity to generate a fluid velocity of 130 μm/s, this research highlights the rapid progress of artificial cilia technology [63]. Rahbar *et al.* fabricated magnetically-actuated cilia using a magnetic nano-composite polymer prepared by doping PDMS with rare-earth magnetic particles. They found that a single artificial cilium was able to mix 90% of the total volume of a control microchamber 122 times faster than passive diffusion.

XI. A. ii. Sensing and Detection Applications

Soft magnetic films are useful in biomedical applications where they can be integrated with flexible electronics to detect magnetic particles. Magnetic nanoparticles have widespread applications in targeted drug delivery, particle tagging, magnetic separation, and enhancing MRI contrast [79]. There needs to be a method to detect and sense these magnetic nanoparticles. Oftentimes, this needs to be done rapidly inside microfluidic channels, highlighting the need for a flexible sensor with the ability to detect magnetic fields [80], [81]

The development and implementation of medical sensors and wearable electronics are greatly enhanced with the help of soft and flexible sensors. These devices can provide real-time information to help with medical diagnosis [82], [83]. Magnetizable films can be used to create sensors for detecting changes in magnetic fields related to physiological signals. For example, Milici *et al.* [84] successfully developed a wearable sensor to detect breathing rate, while Wang *et al.* [85] fabricated a magnetic film sensor to detect magnetic fields of various strengths and polarities.

Artificial cilia-like and hair-like elasto-magnetic structures, in addition to serving as flow, mixing, and transport enhancers, have also been used extensively for a variety of sensing

purposes. Alfadhel *et al.*, for example, employed magnetic nanocomposite based artificial cilia-like structures as tactile sensors for reading braille characters, as shown in [86]. Additionally, Han *et al.* [42] used magnetic molecularly imprinted polymers (MMIPs) based on glutathione (GSH) modified gold-coated Fe_3O_4 NPs to electrochemically detect estradiol.

XI. A. iii. Biomedical Applications

The use of magnetic nanoparticles to enable the actuation of microelectromechanical systems has been repeatedly demonstrated [87]. Magnetic nanoparticles have many biomedical applications. Microscale devices containing magnetic nanoparticles can be wirelessly manipulated using external magnetic fields. Due to the need for biocompatibility, nanoparticles with low toxicity such as iron oxide (Fe_3O_4) are needed. However, because they are so small, these magnetic nanoparticles are superparamagnetic and impart paramagnetic properties instead of ferromagnetic properties to the devices they are embedded in. This is suboptimal because the magnetic susceptibility of paramagnetic materials is low and they do not exhibit spontaneous magnetization [15].

Many ferromagnetic materials are not biocompatible, but soft magnetic films can be used to enable the fabrication of micro-scale medical devices with ferromagnetic properties. This is done by embedding ferromagnetic materials, such as NdFeB, within a biocompatible film material, such as PDMS. The resulting film would be biocompatible while also being ferromagnetic. Iacovacci *et al.* [15] found that while a bare NdFeB film induced toxicity in cultured cancer cells, a PDMS-coated NdFeB film was both biocompatible and cell-adhesive. Being ferromagnetic allows devices to be permanently magnetic and to be controlled with greater speed and precision. Additionally, these devices would also retain the properties of the

soft film material, which includes the soft/compliant nature of the material and the ability to use the fabrication methods of polymers. The use of soft magnetic films would allow the microbots to be used inside the body in various biomedical applications including lab-on-a-chip systems and microsurgery, as well as various minimally invasive procedures such as drug delivery and other targeted therapies, functioning as stents or occlusions, and performing biopsies [88].

Some other biomedical applications for which magnetically actuatable soft films and devices (including magnetic microrobots) have been employed include creating cell transporters and mechanisms for lab-on-a-chip devices. Li *et al.* [54] developed a porous magnetic microbot that can transport and support stem cells. Such stem cell transporters can be actuated to the desired location while also promoting stem cell adhesion, proliferation and differentiation, which indicates the potential for future tissue regeneration capabilities at damaged locations within the body.

XI. A. ix. Miscellaneous Applications

One potential application of hybrid organic-inorganic nanocomposite materials is electromagnetic interference (EMI) shielding. The large variation in alternating current (AC) conductivity exhibited by numerous conducting polymers such as polyaniline (PANI) and polypyrrole (PPy) allows materials composed of these polymers to both transmit and reflect radio-frequency (RF) radiation [89]. The lossy nature of such polymers also contributes to their ability to suppress electromagnetic interference, as opposed to low-loss magnetic and dielectric materials. Soft magnetic films composed of these polymers can be tuned to transmit or reflect RF radiation by applying a voltage bias [89]. There are also potential uses of soft magnetic films in

creating flexible circuit components, from having applications in devices ranging from hard drives to semiconductors.

Research into the utilization of these microstructures and films continue to propel the development and advancement of many locomotion, mixing, electronic, and biomedical technologies and has a plethora of applications including but not exclusive to lab-on-a-chip, sensing and detection technologies, and much more.

XI. B. Future Directions

The large number of intricate thermo-fluidic, colloidal science, and polymer science issues that dictate the fabrication of soft, magnetic inks and films and their application for fabricating multifunctional devices make the topic rich in potential for several future research endeavors in multiple directions. These research questions hover around designing the appropriate combination of the soft (polymeric) materials and the NPs (and issues attributed to these NPs, such as the NP dimensions, functionalizations, concentrations, as well as their interactions with the background polymeric matrix, etc.) that lead to the fabrication of soft, magnetic inks and films with desired processability and capabilities to fabricate devices with desired functionalities.

The manner in which NPs interact in a polymeric matrix has attracted tremendous attention owing to the importance of the topic in fabricating nanocomposites with desired functionalities [90]–[92], [57], [93]. As NP material and their potential applications differ in regards to the varying types of ligands/polymers that functionalize these NPs, exploration is needed to understand such NP-polymer-matrix interactions should be conducted through a

number of approaches such as molecular dynamics (MD) simulations [94]–[98] as well as experimental approaches providing the mechanical properties [99], [100], glass transition temperature [101], [102], thermal conductivity [103], [104] , dielectric constant [104], [105], viscosity and viscoelasticity [106]–[108], and shear thinning properties [109], [110] of these NP-polymer-matrix-based composites (capable of producing the soft, magnetic inks and films of desired properties).

The next important issue is the issue of processability of these materials. The processability includes issues of temperature response of these inks to produce a soft, magnetic film with desired stiffness and magnetizability. Current approaches have invariably relied upon "trial-and-error" approaches in devising such new soft, magnetic inks. A complete paradigm shift will be to approach these problems from a design-driven ink fabrication perspective. In such an approach, a multiscale simulation methodology will be extended to study (1) the interactions between NPs and polymeric materials using atomistic scale simulations, (2) obtain the critical properties of such NP-polymeric systems from these simulations and verify them through experiments, (3) conduct combined thermo-fluidic-mechanical simulations to study the response of these designed inks (aided by the atomistic simulation driven calculation and subsequent experimental verification of the properties of these inks) to the temperature change and confirm if the desired stiffness and magnetizability of such ink has been achieved, and (4) conduct experiments with these designed inks to validate the simulation-predicted findings of the capabilities of these inks in fabricating soft and magnetic films with desired compliance and magnetizability. By conducting "virtual experiments" with a wide range of materials and processing conditions, one could generate a large set of data that could be subjected to machine-learning based evaluation.

The research discussed in this review paper demonstrated that magnetizable films can be manufactured via 3D printing utilizing specific ink compositions. Through this process the films are not only flexible but capable of exhibiting magnetic properties while bent or twisted. To complement this research, future research should focus on confirming these results and test whether successive testing on specimens affect their properties and to what extent. This would demonstrate the films' durability and ability to retain its mechanical and magnetic properties.

Finally, the discovery of new material combinations that enable developing 3D printable, soft, magnetic inks will open up new application potentials of the devices and components fabricated with such inks. These applications include a more precise and sensitive detection of chemicals and generation of flows and vortices (for mixing) at nanoscale (with micron-scale long magnetically responsive soft devices, fabricated through 3D printing tools like nanoscribe), development of more precise therapeutic and detection capabilities, fabricating microbots of very small dimensions that are capable of wide ranging locomotory activities in hitherto unexplored physical spaces (e.g., rubble of a collapsed building or an under-water clogged oil pipeline), and many more.

XII. References

[1] W. Wang, Z. Yao, J. C. Chen, and J. Fang, "Composite elastic magnet films with hard magnetic feature," *J. Micromechanics Microengineering*, vol. 14, no. 10, p. 1321, 2004, doi: 10.1088/0960-1317/14/10/005.

[2] K. Oh, J.-H. Chung, S. Devasia, and J. J. Riley, "Bio-mimetic silicone cilia for microfluidic manipulation," *Lab. Chip*, vol. 9, no. 11, pp. 1561–1566, 2009, doi: 10.1039/B817409A.

[3] A. Shrivastava, *Introduction to plastics engineering*. William Andrew, 2018.

[4] F. Liu, G. Alici, B. Zhang, S. Beirne, and W. Li, "Fabrication and characterization of a magnetic micro-actuator based on deformable Fe-doped PDMS artificial cilium using 3D printing," *Smart Mater. Struct.*, vol. 24, no. 3, p. 035015, 2015, doi: 10.1088/0964-1726/24/3/035015.

[5] F. Pirmoradi, L. Cheng, and M. Chiao, "A magnetic poly(dimethylesiloxane) composite membrane incorporated with uniformly dispersed, coated iron oxide nanoparticles," *J. Micromechanics Microengineering*, vol. 20, no. 1, p. 015032, Dec. 2009, doi: 10.1088/0960-1317/20/1/015032.

[6] N. Banka, Y. L. Ng, and S. Devasia, "Individually controllable magnetic Cilia: Mixing application," *J. Med. Devices*, vol. 11, no. 3, 2017, doi: 10.1115/1.4035984.

[7] S. Zhang, Y. Wang, R. Lavrijsen, P. R. Onck, and J. M. J. den Toonder, "Versatile microfluidic flow generated by moulded magnetic artificial cilia," *Sens. Actuators B Chem.*, vol. 263, pp. 614–624, Jun. 2018, doi: 10.1016/j.snb.2018.01.189.

[8] F. Tsumori, R. Marume, A. Saijou, K. Kudo, T. Osada, and H. Miura, "Metachronal wave of artificial cilia array actuated by applied magnetic field," *Jpn. J. Appl. Phys.*, vol. 55, no. 6S1, p. 06GP19, May 2016, doi: 10.7567/JJAP.55.06GP19.

[9] C.-Y. Chen, C.-Y. Lin, and Y.-T. Hu, "Inducing 3D vortical flow patterns with 2D asymmetric actuation of artificial cilia for high-performance active micromixing," *Exp. Fluids*, vol. 55, no. 7, p. 1765, Jun. 2014, doi: 10.1007/s00348-014-1765-x.

[10] A. R. Shields, B. L. Fiser, B. A. Evans, M. R. Falvo, S. Washburn, and R. Superfine, "Biomimetic cilia arrays generate simultaneous pumping and mixing regimes," *Proc. Natl. Acad. Sci.*, vol. 107, no. 36, pp. 15670–15675, Sep. 2010, doi: 10.1073/pnas.1005127107.

[11] C.-Y. Chen, C.-Y. Chen, C.-Y. Lin, and Y.-T. Hu, "Magnetically actuated artificial cilia for optimum mixing performance in microfluidics," *Lab. Chip*, vol. 13, no. 14, p. 2834, 2013, doi: 10.1039/c3lc50407g.

[12] C.-Y. Chen, L.-Y. Cheng, C.-C. Hsu, and K. Mani, "Microscale flow propulsion through bioinspired and magnetically actuated artificial cilia," *Biomicrofluidics*, vol. 9, no. 3, p. 034105, May 2015, doi: 10.1063/1.4921427.

[13] C.-Y. Chen, T.-C. Chang Chien, K. Mani, and H.-Y. Tsai, "Axial orientation control of zebrafish larvae using artificial cilia," *Microfluid. Nanofluidics*, vol. 20, no. 1, Jan. 2016, doi: 10.1007/s10404-015-1668-z.

[14] P.-Y. Huang, B. Panigrahi, C.-H. Lu, P.-F. Huang, and C.-Y. Chen, "An artificial cilia-based micromixer towards the activation of zebrafish sperms," *Sens. Actuators B Chem.*, vol. 244, pp. 541–548, Jun. 2017, doi: 10.1016/j.snb.2016.12.113.

[15] V. Iacovacci *et al.*, "Polydimethylsiloxane films doped with NdFeB powder: magnetic characterization and potential applications in biomedical engineering and microrobotics," *Biomed. Microdevices*, vol. 17, no. 6, p. 112, Nov. 2015, doi: 10.1007/s10544-015-0024-0.

[16] M. Rahbar, L. Shannon, and B. L. Gray, "Microfluidic active mixers employing ultra-high

aspect-ratio rare-earth magnetic nano-composite polymer artificial cilia," *J. Micromechanics Microengineering*, vol. 24, no. 2, p. 025003, Feb. 2014, doi: 10.1088/0960-1317/24/2/025003.
[17] N. Coq *et al.*, "Collective Beating of Artificial Microcilia," *Phys. Rev. Lett.*, vol. 107, no. 1, Jun. 2011, doi: 10.1103/PhysRevLett.107.014501.
[18] C. Zhang *et al.*, "3D Printing of Functional Magnetic Materials: From Design to Applications," *Adv. Funct. Mater.*, vol. 31, no. 34, p. 2102777, 2021, doi: 10.1002/adfm.202102777.
[19] C. Peters *et al.*, "Superparamagnetic Twist‐Type Actuators with Shape‐Independent Magnetic Properties and Surface Functionalization for Advanced Biomedical Applications," *Adv. Funct. Mater.*, vol. 24, no. 33, pp. 5269–5276, 2014, doi: 10.1002/adfm.201400596.
[20] S. Qi, H. Guo, J. Fu, Y. Xie, M. Zhu, and M. Yu, "3D printed shape-programmable magneto-active soft matter for biomimetic applications," *Compos. Sci. Technol.*, vol. 188, p. 107973, Mar. 2020, doi: 10.1016/j.compscitech.2019.107973.
[21] W. Hu, G. Z. Lum, M. Mastrangeli, and M. Sitti, "Small-scale soft-bodied robot with multimodal locomotion," *Nature*, vol. 554, no. 7690, p. 81, 2018.
[22] Y. Kim, H. Yuk, R. Zhao, S. A. Chester, and X. Zhao, "Printing ferromagnetic domains for untethered fast-transforming soft materials," *Nature*, vol. 558, no. 7709, pp. 274–279, Jun. 2018, doi: 10.1038/s41586-018-0185-0.
[23] W. Ming *et al.*, "Magnetic molecularly imprinted polymers for the fluorescent detection of trace 17β-estradiol in environmental water," *Sens. Actuators B Chem.*, vol. 238, pp. 1309–1315, Jan. 2017, doi: 10.1016/j.snb.2016.09.111.
[24] G. Liu *et al.*, "Competitive fluorescence assay for specific recognition of atrazine by magnetic molecularly imprinted polymer based on Fe3O4-chitosan," *Carbohydr. Polym.*, vol. 137, pp. 75–81, Feb. 2016, doi: 10.1016/j.carbpol.2015.10.062.
[25] X. Li, X. Wang, L. Li, H. Duan, and C. Luo, "Electrochemical sensor based on magnetic graphene oxide@gold nanoparticles-molecular imprinted polymers for determination of dibutyl phthalate," *Talanta*, vol. 131, pp. 354–360, Jan. 2015, doi: 10.1016/j.talanta.2014.07.028.
[26] A. L. Medina-Castillo, G. Mistlberger, J. F. Fernandez-Sanchez, A. Segura-Carretero, I. Klimant, and A. Fernandez-Gutierrez, "Novel Strategy To Design Magnetic, Molecular Imprinted Polymers with Well-Controlled Structure for the Application in Optical Sensors," *Macromolecules*, vol. 43, no. 1, pp. 55–61, Jan. 2010, doi: 10.1021/ma902095s.
[27] S. Khaderi, J. Hussong, J. Westerweel, J. den Toonder, and P. Onck, "Fluid propulsion using magnetically-actuated artificial cilia – experiments and simulations," *RSC Adv.*, vol. 3, no. 31, pp. 12735–12742, Jul. 2013, doi: 10.1039/C3RA42068J.
[28] S. N. Khaderi *et al.*, "Magnetically-actuated artificial cilia for microfluidic propulsion," *Lab. Chip*, vol. 11, no. 12, pp. 2002–2010, 2011, doi: 10.1039/C0LC00411A.
[29] A. A. Lahcen, A. A. Baleg, P. Baker, E. Iwuoha, and A. Amine, "Synthesis and electrochemical characterization of nanostructured magnetic molecularly imprinted polymers for 17-β-Estradiol determination," *Sens. Actuators B Chem.*, vol. 241, pp. 698–705, Mar. 2017, doi: 10.1016/j.snb.2016.10.132.
[30] H. Li, G. Go, S. Y. Ko, J.-O. Park, and S. Park, "Magnetic actuated pH-responsive hydrogel-based soft micro-robot for targeted drug delivery," *Smart Mater. Struct.*, vol. 25, no. 2, p. 027001, Jan. 2016, doi: 10.1088/0964-1726/25/2/027001.

[31] M. P. Wolf, G. B. Salieb-Beugelaar, and P. Hunziker, “PDMS with designer functionalities—Properties, modifications strategies, and applications,” *Prog. Polym. Sci.*, vol. 83, pp. 97–134, Aug. 2018, doi: 10.1016/j.progpolymsci.2018.06.001.
[32] K. Villa, L. Krejčová, F. Novotný, Z. Heger, Z. Sofer, and M. Pumera, “Cooperative Multifunctional Self-Propelled Paramagnetic Microrobots with Chemical Handles for Cell Manipulation and Drug Delivery,” *Adv. Funct. Mater.*, vol. 28, no. 43, p. 1804343, 2018, doi: 10.1002/adfm.201804343.
[33] C. Peters, M. Hoop, S. Pané, B. J. Nelson, and C. Hierold, “Degradable Magnetic Composites for Minimally Invasive Interventions: Device Fabrication, Targeted Drug Delivery, and Cytotoxicity Tests,” *Adv. Mater.*, vol. 28, no. 3, pp. 533–538, 2016, doi: 10.1002/adma.201503112.
[34] G.-H. Yao, R.-P. Liang, C.-F. Huang, Y. Wang, and J.-D. Qiu, “Surface Plasmon Resonance Sensor Based on Magnetic Molecularly Imprinted Polymers Amplification for Pesticide Recognition,” *Anal. Chem.*, vol. 85, no. 24, pp. 11944–11951, Dec. 2013, doi: 10.1021/ac402848x.
[35] Z. Ji, C. Yan, B. Yu, X. Wang, and F. Zhou, “Multimaterials 3D Printing for Free Assembly Manufacturing of Magnetic Driving Soft Actuator,” *Adv. Mater. Interfaces*, vol. 4, no. 22, p. 1700629, 2017, doi: 10.1002/admi.201700629.
[36] F. Lu *et al.*, “Flow injection chemiluminescence sensor based on core–shell magnetic molecularly imprinted nanoparticles for determination of sulfadiazine,” *Anal. Chim. Acta*, vol. 718, pp. 84–91, Mar. 2012, doi: 10.1016/j.aca.2011.12.054.
[37] S. Fusco *et al.*, “Shape-Switching Microrobots for Medical Applications: The Influence of Shape in Drug Delivery and Locomotion,” *ACS Appl. Mater. Interfaces*, vol. 7, no. 12, pp. 6803–6811, Apr. 2015, doi: 10.1021/acsami.5b00181.
[38] J. V. I. Timonen, C. Johans, K. Kontturi, A. Walther, O. Ikkala, and R. H. A. Ras, “A Facile Template-Free Approach to Magnetodriven, Multifunctional Artificial Cilia,” *ACS Appl. Mater. Interfaces*, vol. 2, no. 8, pp. 2226–2230, Aug. 2010, doi: 10.1021/am100244x.
[39] R. U. Hassan, S. Jo, and J. Seok, “Fabrication of a functionally graded and magnetically responsive shape memory polymer using a 3D printing technique and its characterization,” *J. Appl. Polym. Sci.*, vol. 135, no. 11, p. 45997, 2018, doi: 10.1002/app.45997.
[40] M. Rahbar, S. Seyfollahi, A. Khosla, B. L. Gray, and L. Shannon, “Fabrication Process for Electromagnetic Actuators Compatible with Polymer Based Microfluidic Devices,” *ECS Trans.*, vol. 41, no. 20, p. 7, May 2012, doi: 10.1149/1.3687433.
[41] Q. Guo, X. Teng, S. Rahman, and H. Yang, “Patterned Langmuir−Blodgett Films of Monodisperse Nanoparticles of Iron Oxide Using Soft Lithography,” *J. Am. Chem. Soc.*, vol. 125, no. 3, pp. 630–631, Jan. 2003, doi: 10.1021/ja0275764.
[42] Q. Han, X. Shen, W. Zhu, C. Zhu, X. Zhou, and H. Jiang, “Magnetic sensing film based on Fe3O4@Au-GSH molecularly imprinted polymers for the electrochemical detection of estradiol,” *Biosens. Bioelectron.*, vol. 79, pp. 180–186, May 2016, doi: 10.1016/j.bios.2015.12.017.
[43] J. A. Lewis, “Direct Ink Writing of 3D Functional Materials,” *Adv. Funct. Mater.*, vol. 16, no. 17, pp. 2193–2204, Nov. 2006, doi: 10.1002/adfm.200600434.
[44] S.-G. Cho, K.-W. Jeon, J. Kim, K. H. Kim, and J. Kim, “Synthesis and ferromagnetic properties of magnetic ink for direct printing,” *IEEE Trans. Magn.*, vol. 47, no. 10, pp. 3157–3159, 2011.
[45] L. Sun and Y. Zheng, “Bio-inspired artificial cilia with magnetic dynamic properties,”

Front. Mater. Sci., vol. 9, no. 2, pp. 178–184, Jun. 2015, doi: 10.1007/s11706-015-0291-y.
[46] C.-Y. Chen, C.-C. Hsu, K. Mani, and B. Panigrahi, "Hydrodynamic influences of artificial cilia beating behaviors on micromixing," *Chem. Eng. Process. Process Intensif.*, vol. 99, pp. 33–40, Jan. 2016, doi: 10.1016/j.cep.2015.10.023.
[47] J. Belardi, N. Schorr, O. Prucker, and J. Rühe, "Artificial Cilia: Generation of Magnetic Actuators in Microfluidic Systems," *Adv. Funct. Mater.*, vol. 21, no. 17, pp. 3314–3320, Jul. 2011, doi: https://doi.org/10.1002/adfm.201100787.
[48] F. Fahrni, M. W. J. Prins, and L. J. van IJzendoorn, "Micro-fluidic actuation using magnetic artificial cilia," *Lab. Chip*, no. 23, pp. 3413–3421, 2009, doi: 10.1039/b908578e.
[49] S. Hanasoge, M. Ballard, P. J. Hesketh, and A. Alexeev, "Asymmetric motion of magnetically actuated artificial cilia," *Lab. Chip*, vol. 17, no. 18, pp. 3138–3145, Sep. 2017, doi: 10.1039/C7LC00556C.
[50] S. Hanasoge, P. J. Hesketh, and A. Alexeev, "Microfluidic pumping using artificial magnetic cilia," *Microsyst. Nanoeng.*, vol. 4, no. 1, Dec. 2018, doi: 10.1038/s41378-018-0010-9.
[51] Y. Wang, J. den Toonder, R. Cardinaels, and P. Anderson, "A continuous roll-pulling approach for the fabrication of magnetic artificial cilia with microfluidic pumping capability," *Lab. Chip*, vol. 16, no. 12, pp. 2277–2286, 2016, doi: 10.1039/C6LC00531D.
[52] I. Cooperstein *et al.*, "Hybrid Materials for Functional 3D Printing," *Adv. Mater. Interfaces*, vol. 5, no. 22, p. 1800996, 2018, doi: 10.1002/admi.201800996.
[53] V. Iacovacci, G. Lucarini, L. Ricotti, P. Dario, P. E. Dupont, and A. Menciassi, "Untethered magnetic millirobot for targeted drug delivery," *Biomed. Microdevices*, vol. 17, no. 3, p. 63, May 2015, doi: 10.1007/s10544-015-9962-9.
[54] J. Li *et al.*, "Development of a magnetic microrobot for carrying and delivering targeted cells," *Sci. Robot.*, vol. 3, no. 19, Jun. 2018, doi: 10.1126/scirobotics.aat8829.
[55] T.-Y. Huang *et al.*, "3D Printed Microtransporters: Compound Micromachines for Spatiotemporally Controlled Delivery of Therapeutic Agents," *Adv. Mater.*, vol. 27, no. 42, Nov. 2015, doi: 10.1002/adma.201503095.
[56] D. J. Thomas, Z. Tehrani, and B. Redfearn, "3-D printed composite microfluidic pump for wearable biomedical applications," *Addit. Manuf.*, vol. 9, pp. 30–38, Jan. 2016, doi: 10.1016/j.addma.2015.12.004.
[57] S. M. Ashrafi-Shahri, F. Ravari, and D. Seifzadeh, "Smart organic/inorganic sol-gel nanocomposite containing functionalized mesoporous silica for corrosion protection," *Prog. Org. Coat.*, vol. 133, pp. 44–54, Aug. 2019, doi: 10.1016/j.porgcoat.2019.04.038.
[58] A. A. Novakova *et al.*, "Magnetic properties of polymer nanocomposites containing iron oxide nanoparticles," *J. Magn. Magn. Mater.*, vol. 258–259, pp. 354–357, Mar. 2003, doi: 10.1016/S0304-8853(02)01062-4.
[59] Y. Bando, S. Horii, and T. Takada, "Reactive Condensation and Magnetic Properties of Iron Oxide Films," *Jpn. J. Appl. Phys.*, vol. 17, no. 6, p. 1037, Jun. 1978, doi: 10.1143/JJAP.17.1037.
[60] P. Dankers, "Relationship between median destructive field and remanent coercive forces for dispersed natural magnetite, titanomagnetite and hematite," *Geophys. J. Int.*, vol. 64, no. 2, pp. 447–461, Feb. 1981, doi: 10.1111/j.1365-246X.1981.tb02676.x.
[61] J. M. J. den Toonder and P. R. Onck, "Microfluidic manipulation with artificial/bioinspired cilia," *Trends Biotechnol.*, vol. 31, no. 2, pp. 85–91, Feb. 2013, doi: 10.1016/j.tibtech.2012.11.005.

[62] A. Babataheri, M. Roper, M. Fermigier, and O. du Roure, “Tethered fleximags as artificial cilia,” *J. Fluid Mech.*, vol. 678, pp. 5–13, Jul. 2011, doi: https://doi.org/10.1017/S002211201100005X.
[63] J. Hussong, N. Schorr, J. Belardi, O. Prucker, J. Rühe, and J. Westerweel, “Experimental investigation of the flow induced by artificial cilia,” *Lab. Chip*, vol. 11, no. 12, p. 2017, 2011, doi: 10.1039/c0lc00722f.
[64] Y. Ariake *et al.*, “The Thickness Dependence of Soft Magnetic Properties of (FeCo)-Al Alloy Thin Films,” *IEEE Trans. Magn.*, vol. 53, no. 11, pp. 1–4, Nov. 2017, doi: 10.1109/TMAG.2017.2700320.
[65] Y. K. Kim and M. Oliveria, “Magnetic properties of sputtered Fe thin films: Processing and thickness dependence,” *J. Appl. Phys.*, vol. 74, no. 2, pp. 1233–1241, Jul. 1993, doi: 10.1063/1.354926.
[66] M. Liu, L. Qian, C. Yu, G. Xiao, and R. H. Hurt, “An all-inorganic, fully dense, stretchable ceramic magnetic film,” *Nanoscale Adv.*, vol. 3, no. 3, pp. 800–804, Feb. 2021, doi: 10.1039/D0NA00949K.
[67] J. Liang *et al.*, “Flexible, Magnetic, and Electrically Conductive Graphene/Fe3O4 Paper and Its Application for Magnetic-Controlled Switches,” *J. Phys. Chem. C*, vol. 114, no. 41, pp. 17465–17471, Oct. 2010, doi: 10.1021/jp105629r.
[68] Y. Zhang *et al.*, “Flexible Quasi-Two-Dimensional CoFe2O4 Epitaxial Thin Films for Continuous Strain Tuning of Magnetic Properties,” *ACS Nano*, vol. 11, no. 8, pp. 8002–8009, Aug. 2017, doi: 10.1021/acsnano.7b02637.
[69] J. Zhang, Y. Guo, W. Hu, R. H. Soon, Z. S. Davidson, and M. Sitti, “Liquid Crystal Elastomer-Based Magnetic Composite Films for Reconfigurable Shape-Morphing Soft Miniature Machines,” *Adv. Mater.*, vol. 33, no. 8, p. 2006191, 2021, doi: 10.1002/adma.202006191.
[70] P. Dickey, “Convention on the Rights of Persons with Disabilities,” *U. N.*, p. 28, 2006.
[71] “What is meant by ‘accessible information’? | ICT4IAL,” *ICT for Information Accessibility in Learning*. https://www.ict4ial.eu/what-meant-accessible-information (accessed Mar. 15, 2022).
[72] S. Day, S. Rennie, D. Luo, and J. D. Tucker, “Open to the public: paywalls and the public rationale for open access medical research publishing,” *Res. Involv. Engagem.*, vol. 6, no. 1, p. 8, Feb. 2020, doi: 10.1186/s40900-020-0182-y.
[73] B. K. Gale, M. A. Eddings, S. O. Sundberg, A. Hatch, J. Kim, and T. Ho, “Low-Cost MEMS Technologies,” in *Comprehensive Microsystems*, Y. B. Gianchandani, O. Tabata, and H. Zappe, Eds. Oxford: Elsevier, 2008, pp. 341–378. doi: 10.1016/B978-044452190-3.00011-2.
[74] D. A. Bruzewicz, M. Reches, and G. M. Whitesides, “Low-Cost Printing of PDMS Barriers to Define Microchannels in Paper,” *Anal. Chem.*, vol. 80, no. 9, pp. 3387–3392, May 2008, doi: 10.1021/ac702605a.
[75] K. E. Peyer, L. Zhang, and B. J. Nelson, “Bio-inspired magnetic swimming microrobots for biomedical applications,” *Nanoscale*, vol. 5, no. 4, pp. 1259–1272, 2013, doi: 10.1039/C2NR32554C.
[76] S. Kim, S. Lee, J. Lee, B. J. Nelson, L. Zhang, and H. Choi, “Fabrication and manipulation of ciliary microrobots with non-reciprocal magnetic actuation,” *Sci. Rep.*, vol. 6, p. 30713, 2016, doi: 10.1038/srep30713.
[77] L. Zhang, J. J. Abbott, L. Dong, B. E. Kratochvil, D. Bell, and B. J. Nelson, “Artificial

bacterial flagella: Fabrication and magnetic control," *Appl. Phys. Lett.*, vol. 94, no. 6, p. 064107, Feb. 2009, doi: 10.1063/1.3079655.
[78] S. Sareh, J. Rossiter, A. Conn, K. Drescher, and R. E. Goldstein, "Swimming like algae: biomimetic soft artificial cilia," *J. R. Soc. Interface*, vol. 10, no. 78, p. 20120666, 2013, doi: 10.1098/rsif.2012.0666.
[79] Q. A. Pankhurst, J. Connolly, S. K. Jones, and J. Dobson, "Applications of magnetic nanoparticles in biomedicine," *J. Phys. Appl. Phys.*, vol. 36, no. 13, pp. R167–R181, Jun. 2003, doi: 10.1088/0022-3727/36/13/201.
[80] Y.-W. Liu, Q.-F. Zhan, and R.-W. Li, "Fabrication, properties, and applications of flexible magnetic films," *Chin. Phys. B*, vol. 22, no. 12, p. 127502, Dec. 2013, doi: 10.1088/1674-1056/22/12/127502.
[81] I. Mönch *et al.*, "Rolled-Up Magnetic Sensor: Nanomembrane Architecture for In-Flow Detection of Magnetic Objects," *ACS Nano*, vol. 5, no. 9, pp. 7436–7442, Sep. 2011, doi: 10.1021/nn202351j.
[82] X. Wang, Z. Liu, and T. Zhang, "Flexible Sensing Electronics for Wearable/Attachable Health Monitoring," *Small*, vol. 13, no. 25, p. 1602790, 2017, doi: 10.1002/smll.201602790.
[83] C. Wang, K. Xia, H. Wang, X. Liang, Z. Yin, and Y. Zhang, "Advanced Carbon for Flexible and Wearable Electronics," *Adv. Mater.*, vol. 31, no. 9, p. 1801072, 2019, doi: 10.1002/adma.201801072.
[84] S. Milici, A. Guillen, R. Villarino, D. Girbau, and M. Magnarosa, "Wireless Wearable Magnetometer-Based Sensor for Sleep Quality Monitoring", [Online]. Available: https://doi.org/10.1109/JSEN.2018.2791400
[85] Z. Wang *et al.*, "Highly Sensitive Flexible Magnetic Sensor Based on Anisotropic Magnetoresistance Effect," *Adv. Mater.*, vol. 28, no. 42, pp. 9370–9377, 2016, doi: 10.1002/adma.201602910.
[86] A. Alfadhel, M. A. Khan, S. Cardoso de Freitas, and J. Kosel, "Magnetic Tactile Sensor for Braille Reading," *IEEE Sens. J.*, vol. 16, no. 24, pp. 8700–8705, Dec. 2016, doi: 10.1109/JSEN.2016.2558599.
[87] F. Dragomir and O. E. Dragomir, "Microrobotics: Present, challenges, perspectives," in *2014 IEEE International Conference on Robotics and Biomimetics (ROBIO 2014)*, Dec. 2014, pp. 1904–1909. doi: 10.1109/ROBIO.2014.7090614.
[88] B. J. Nelson, I. K. Kaliakatsos, and J. J. Abbott, "Microrobots for Minimally Invasive Medicine," *Annu. Rev. Biomed. Eng.*, vol. 12, no. 1, pp. 55–85, Jul. 2010, doi: 10.1146/annurev-bioeng-010510-103409.
[89] J. Gass, P. Poddar, J. Almand, S. Srinath, and H. Srikanth, "Superparamagnetic Polymer Nanocomposites with Uniform Fe3O4 Nanoparticle Dispersions," *Adv. Funct. Mater.*, vol. 16, no. 1, Dec. 2005, doi: 10.1002/adfm.200500335.
[90] E. Tanasa *et al.*, "Novel Nanocomposites Based on Functionalized Magnetic Nanoparticles and Polyacrylamide: Preparation and Complex Characterization," *Nanomaterials*, vol. 9, no. 10, 2019, doi: 10.3390/nano9101384.
[91] J. Li, J. Claude, L. E. Norena-Franco, S. I. Seok, and Q. Wang, "Electrical Energy Storage in Ferroelectric Polymer Nanocomposites Containing Surface-Functionalized BaTiO3 Nanoparticles," *Chem. Mater.*, vol. 20, no. 20, pp. 6304–6306, Oct. 2008, doi: 10.1021/cm8021648.
[92] Z. Guo, T. Pereira, O. Choi, Y. Wang, and H. T. Hahn, "Surface functionalized alumina

nanoparticle filled polymeric nanocomposites with enhanced mechanical properties," *J. Mater. Chem.*, vol. 16, no. 27, pp. 2800–2808, 2006, doi: 10.1039/B603020C.
[93] N. Nasrollahi, S. Aber, V. Vatanpour, and N. M. Mahmoodi, "The effect of amine functionalization of CuO and ZnO nanoparticles used as additives on the morphology and the permeation properties of polyethersulfone ultrafiltration nanocomposite membranes," *Compos. Part B Eng.*, vol. 154, pp. 388–409, Dec. 2018, doi: 10.1016/j.compositesb.2018.09.027.
[94] S. Chakraborty, F. C. H. Lim, and J. Ye, "Achieving an Optimal Tg Change by Elucidating the Polymer–Nanoparticle Interface: A Molecular Dynamics Simulation Study of the Poly(vinyl alcohol)–Silica Nanocomposite System," *J. Phys. Chem. C*, vol. 123, no. 39, pp. 23995–24006, Oct. 2019, doi: 10.1021/acs.jpcc.9b05545.
[95] J. Liu, Y. Gao, D. Cao, L. Zhang, and Z. Guo, "Nanoparticle Dispersion and Aggregation in Polymer Nanocomposites: Insights from Molecular Dynamics Simulation," *Langmuir*, vol. 27, no. 12, pp. 7926–7933, Jun. 2011, doi: 10.1021/la201073m.
[96] X.-M. Jia, H.-J. Qian, and Z.-Y. Lu, "The interfacial structure and dynamics in a polymer nanocomposite containing small attractive nanoparticles: a full atomistic molecular dynamics simulation study," *Phys. Chem. Chem. Phys.*, vol. 22, no. 20, pp. 11400–11408, May 2020, doi: 10.1039/D0CP00799D.
[97] Z. Zheng *et al.*, "Molecular Dynamics Simulation Study of Polymer Nanocomposites with Controllable Dispersion of Spherical Nanoparticles," *J. Phys. Chem. B*, vol. 121, no. 43, pp. 10146–10156, Nov. 2017, doi: 10.1021/acs.jpcb.7b06482.
[98] M. Nematollahi, A. Jalali-Arani, K. Golzar, and H. Modarress, "Investigation of nanoparticle–polymer interaction in bio-based nanosilica-filled PLA/NR nanocomposites: molecular dynamics simulation," *J. Mol. Model.*, vol. 26, no. 9, p. 230, Aug. 2020, doi: 10.1007/s00894-020-04431-3.
[99] M. A. Maghsoudlou, R. Barbaz Isfahani, S. Saber-Samandari, and M. Sadighi, "Effect of interphase, curvature and agglomeration of SWCNTs on mechanical properties of polymer-based nanocomposites: Experimental and numerical investigations," *Compos. Part B Eng.*, vol. 175, p. 107119, Oct. 2019, doi: 10.1016/j.compositesb.2019.107119.
[100] M. Heydari-Meybodi, S. Saber-Samandari, and M. Sadighi, "A new approach for prediction of elastic modulus of polymer/nanoclay composites by considering interfacial debonding: Experimental and numerical investigations," *Compos. Sci. Technol.*, vol. 117, pp. 379–385, Sep. 2015, doi: 10.1016/j.compscitech.2015.07.014.
[101] P. Rittigstein and J. M. Torkelson, "Polymer–nanoparticle interfacial interactions in polymer nanocomposites: Confinement effects on glass transition temperature and suppression of physical aging," *J. Polym. Sci. Part B Polym. Phys.*, vol. 44, no. 20, pp. 2935–2943, 2006, doi: https://doi.org/10.1002/polb.20925.
[102] Y. Sun, Z. Zhang, K.-S. Moon, and C. P. Wong, "Glass transition and relaxation behavior of epoxy nanocomposites," *J. Polym. Sci. Part B Polym. Phys.*, vol. 42, no. 21, pp. 3849–3858, 2004, doi: https://doi.org/10.1002/polb.20251.
[103] A. Tessema *et al.*, "Effect of filler loading, geometry, dispersion and temperature on thermal conductivity of polymer nanocomposites," *Polym. Test.*, vol. 57, pp. 101–106, Feb. 2017, doi: 10.1016/j.polymertesting.2016.11.015.
[104] X. Huang, P. Jiang, and L. Xie, "Ferroelectric polymer/silver nanocomposites with high dielectric constant and high thermal conductivity," *Appl. Phys. Lett.*, vol. 95, no. 24, p. 242901, Dec. 2009, doi: 10.1063/1.3273368.

[105] J. Lu, K.-S. Moon, and C. P. Wong, “Silver/polymer nanocomposite as a high-kpolymer matrix for dielectric composites with improved dielectric performance,” *J. Mater. Chem.*, vol. 18, no. 40, pp. 4821–4826, Oct. 2008, doi: 10.1039/B807566B.
[106] A. Tuteja, P. M. Duxbury, and M. E. Mackay, “Multifunctional Nanocomposites with Reduced Viscosity,” *Macromolecules*, vol. 40, no. 26, pp. 9427–9434, Dec. 2007, doi: 10.1021/ma071313i.
[107] X. Shi, M. K. Hassanzadeh-Aghdam, and R. Ansari, “Viscoelastic analysis of silica nanoparticle-polymer nanocomposites,” *Compos. Part B Eng.*, vol. 158, pp. 169–178, Feb. 2019, doi: 10.1016/j.compositesb.2018.09.084.
[108] P. Bindu and S. Thomas, “Viscoelastic Behavior and Reinforcement Mechanism in Rubber Nanocomposites in the Vicinity of Spherical Nanoparticles,” *J. Phys. Chem. B*, vol. 117, no. 41, pp. 12632–12648, Oct. 2013, doi: 10.1021/jp4039489.
[109] X.-L. Xie *et al.*, “Rheological and mechanical properties of PVC/CaCO3 nanocomposites prepared by in situ polymerization,” *Polymer*, vol. 45, no. 19, pp. 6665–6673, Sep. 2004, doi: 10.1016/j.polymer.2004.07.045.
[110] X. Yan *et al.*, “Magnetic Polystyrene Nanocomposites Reinforced with Magnetite Nanoparticles,” *Macromol. Mater. Eng.*, vol. 299, no. 4, pp. 485–494, 2014, doi: https://doi.org/10.1002/mame.201300208.